Distribution Agreement

In presenting this thesis as a partial fulfillment of the requirements for a degree from Emory University, I hereby grant to Emory University and its agents the non-exclusive license to archive, make accessible, and display my thesis in whole or in part in all forms of media, now or hereafter now, including display on the World Wide Web. I understand that I may select some access restrictions as part of the online submission of this thesis. I retain all ownership rights to the copyright of the thesis. I also retain the right to use in future works (such as articles or books) all or part of this thesis.

Michael Mu   April 14, 2020

LCMT-1 is an essential component of neuronal development

by

Michael Mu

David C. Pallas

Adviser

Biology

David C. Pallas

Adviser

Anita H. Corbett

Committee Member

Arthur W. English

Committee Member

2020

LCMT-1 is an essential component of neuronal development

By

Michael Mu

David C. Pallas

Adviser

An abstract of
a thesis submitted to the Faculty of Emory College of Arts and Sciences
of Emory University in partial fulfillment
of the requirements of the degree of
Bachelor of Science with Honors

Biology

2020

Abstract

LCMT-1 is an essential component of neuronal development

By Michael Mu

Protein phosphatase 2A (PP2A) is an important ubiquitous heterotrimeric protein phosphatase that participates in many important biochemical processes and pathways by regulating the phosphorylation state of numerous substrates. Global knockout (KO) of the gene encoding leucine carboxyl methyltransferase-1 (LCMT-1), a methyltransferase that regulates the stable formation of a subset of PP2A heterotrimers, results in late gestational embryonic lethality in mice [Lee & Pallas, 2018]. The neuronal consequences of LCMT-1 loss have only begun to be investigated, as have its potential impacts on the development of Alzheimer's Disease (AD) pathology. In this study, we find tau hyperphosphorylation at important AD-correlated sites in global *Lcmt-1* KO embryo brains. We also find that cultured hippocampal neurons from global *Lcmt-1* KO embryos display stunted neurite outgrowth and abnormal neuronal polarity. Further, using a n*estin-Cre*-mediated neuronal-conditional *Lcmt-1* knockout (cKO) mouse model, we find that neuronal loss of LCMT-1 results in perinatal lethality on average 22 hours after birth, likely due at least in part to an inability to feed. In P0 *Lcmt-1* cKO pups, we also find evidence for hyperphosphorylation of tau at the Tau-1 antibody epitope and an increase in amount and possibly phosphorylation of an unknown isoform or truncated form of tau. Finally, using a neuronal YFP-expressing mouse model, we find that *Lcmt-1* cKO hippocampal CA pyramidal cell layer neurons are reduced in number, and consistent with this, there is an apparent thinning of these cell layers. Thus, LCMT-1 has critical roles in neuronal development and in prevention of AD-related changes in tau phosphorylation.

LCMT-1 is an essential component of neuronal development

By

Michael Mu

David C. Pallas

Adviser

A thesis submitted to the Faculty of Emory College of Arts and Sciences
of Emory University in partial fulfillment
of the requirements of the degree of
Bachelor of Science with Honors

Biology

2020

Table of Contents

LCMT-1 is an essential component of neuronal development

Introduction

Protein phosphatase 2A (PP2A) is a heterotrimeric protein phosphatase that regulates numerous

substrates through dephosphorylation. PP2A consists of an A scaffold subunit, a B regulatory

subunit, and a C catalytic subunit. While mammals have two genes each (α, β) encoding the A

and C subunits, there are many genes encoding the B regulatory subunits. Thus, PP2A

heterotrimers are mostly differentiated from each other by the particular B subunit isoform they

possess, of which there are 4 subfamilies: B (PPP2R2), B' (PPP2R5), B'' (PPP2R3), and B'''

(striatin family). PP2A has been found to have widespread and crucial roles in many cellular

processes, including cell cycle, apoptosis and tumor suppression, and proper cardiac and nervous

tissue function [Wlodarchak & Xing, 2016]. Furthermore, PP2A has been implicated in many

important biochemical pathways, including the Wnt, mTOR, and MAPK pathways [Wlodarchak

& Xing, 2016]. Many studies have implicated PP2A in proper brain function, with the reduction

of PP2A noted in several common diseases. For example, mRNA expression of PP2A has been

shown to be decreased substantially in the hippocampus of Alzheimer's Disease (AD) patient

brains [Vogelsberg-Ragaglia et al., 2001].

Leucine carboxyl methyltransferase-1 (LCMT-1) is an enzyme that methylates PP2A

catalytic subunit (PP2Ac), as well as the catalytic subunits of the other PP2A family phosphatases,

protein phosphatase 4 (PP4) and protein phosphatase 6 (PP6) [Hwang et al., 2016]. In the case of

PP2A and PP4, this modification has been shown to enable formation of certain functional PP2A

or PP4 heterotrimers, termed "methylation-dependent" heterotrimers. This methylation is

reversible, with demethylation of PP2A and likely PP4 and PP6 carried out by a protein

methylesterase, PME-1 [Ogris et al., 1999]. Thus, targeting PP2A family phosphatase methylation is a potential therapeutic strategy.

Mice with the *Lcmt-1* gene knocked out in all cells (global KO) die before birth due to defects in several tissues [Lee & Pallas, 2018]. As for PP2A, LCMT-1 has been linked to neuronal diseases. However, studies have only correlated PP2A and LCMT-1 downregulation with such neuronal diseases [Park et al., 2016, Park et al., 2018, Vogelsberg-Ragaglia et al., 2001] or only studied effects *in vitro* [Yang et al., 2016, Sontag et al., 2013, Deters et al., 2009]. For example, decreased levels of methylated PP2A C subunit have been found in postmortem tauopathy and AD brains [Park et al., 2018], and knockdown of LCMT-1 in neuroblastoma cells has been found to decrease neurite outgrowth [Sontag et al., 2010] and decrease association of PP2A with tau protein at the plasma membrane [Sontag et al., 2013]. Direct involvement of LCMT-1 in the development of AD pathology would provide the grounds for the pursuit of therapeutic drugs.

An important area of investigation in this area of research is the study of tau. Tau is a microtubule-associated protein (MAP) that is heavily implicated in the pathology of AD through its hyperphosphorylation-induced formation of neurofibrillary tangles (NFTs) [Pîrşcoveanu et al., 2017]. However, tau may also regulate normal neuronal function as MAPs bind to tubulin and microtubules in order to facilitate the formation of cytoskeletal networks, a process integral to neurite outgrowth and maintenance. Tau is a known target of PP2A [Martin et al., 2013]. Additionally, a few studies have linked LCMT-1 and PP2A methylation to tau phosphorylation in cells [Yang et al., 2016; Wang et al., 2015]. Finally, one study overexpressing PME-1 in adult mouse forebrain showed increased tau phosphorylation at several sites [Nicholls et al., 2016]. It remains to be seen whether this effect can occur developmentally.

In order to investigate the relationship between LCMT-1 and proteins like tau, as well as study the role of LCMT-1 in the nervous system, we have utilized our global LCMT-1 KO model and a conditional knockout (cKO) using the Cre-*loxP* system. Our results reveal differences between global and conditional LCMT-1 knockout and start painting a picture of the ramifications of neuronal-specific LCMT-1 knockout without extrinsic effects. In both systems, we find evidence of multiple neuronal defects, thus revealing novel roles of LCMT-1 in neuronal systems.

Materials and Methods

This research was reviewed and approved by the Emory University Institutional Animal Care and Use Committee (IACUC).

Gene-trap global LCMT-1 KO mice: The same gene-trap-mediated global knockout system was used from our previously published work [Lee and Pallas, 2007]. Briefly, a gene trap was inserted in the first intron of *lcmt-1* in stem cells, which were then injected into developing C57BL/6 embryos. Resulting mice born from foster mothers were backcrossed to recreate the homogeneous line.

Neuronal-conditional LCMT-1 KO mice: Nestin-Cre (Jackson Laboratories, B6.Cg-Tg(Nes-Cre)1Kln/J, Stock No. 003771) mice were used. This knockout method is described in Figure S1. Cre-*loxP*-mediated conditional LCMT-1 knockout (cKO) mice were created by breeding "floxed" (exon 3 of LCMT-1 flanked by *loxP* sites) LCMT-1 mice with mice expressing *nestin-Cre*. *Nestin-Cre* starts expressing Cre recombinase in mid to late brain development, starting around E14.5 and becoming sufficient for widespread induction of recombination by E17.5 [Liang et al., 2012]. *Nestin-Cre* expression occurs particularly in the neural stem cells and intermediate neural progenitor cells which differentiate into almost all neurons and glial cells of the brain [Bernal &

Arranz, 2018]. However, some expression also occurs in the bone marrow, as well as a few isolated kidney and heart cells [Bernal & Arranz, 2018]. The presence of the *nestin-Cre* itself has been shown to result in hypopituitarism, growth retardation, impaired fear response, and a metabolic phenotype [Declercq et al., 2015].

YFP mice: Thy1-YFP (Jackson Laboratories, B6.Cg-Tg(Thy1-YFP)16Jrs/J, Stock No. 003709) mice, also known as Thy-1 YFP-16, were gifts of Dr. Yue Feng in the Emory Department of Pharmacology. These transgenic mice express yellow fluorescent protein in predominantly motor and sensory neurons, and particularly provide a strong marker for axons. Expression starts in mid-gestation and continues through adulthood. YFP-expressing mice were bred with *nestin-Cre* cKO mice to combine both systems and allow for imaging of cKO neurons.

Genotyping: DNA was extracted from tails or other tissue that were digested with proteinase-K overnight. The DNA extraction procedure involved digestion overnight in a 55°C water bath in tail lysis buffer (100 mM Tris-HCl pH 8.5, 5 mM EDTA, 0.2% SDS, 200 mM NaCl, 100 μg/ml proteinase K), centrifugation to separate out undigested fur tissue, isopropanol-precipitation of DNA, and resuspension of DNA in deionized water. Primers detecting the LCMT-1 gene trap, knockout [Lee et al., 2018], the Cre gene, YFP, or flanking one of the *loxP* sites (results in a difference in product size depending on the presence or absence of the loxP site) were used to perform PCR. PCR was performed using Promega Green GoTaq® reaction buffer and ProMega GoTaq® DNA Polymerase according the manufacturer's instructions. All embryos, pups, and adult mice were genotyped using PCR with primers specific to each genetic modification followed by ethidium bromide-stained gel electrophoresis. PCR details are as follows:

Lcmt-1 gene trap: *Lcmt-1* PCR using one forward primer and two reverse primers is described in our previous work [Lee et al., 2018]. A wild-type *Lcmt-1* allele generates a ∼200-bp

fragment of endogenous *Lcmt-1*, whereas a gene-trap knockout allele of *Lcmt-1* generates a ~250-bp product between the *Lcmt-1* intron 1 and LacZ in the pT1βgeo gene trap cassette.

Cre: 30 cycles of PCR (95°C for 30 s; 54°C for 30 s; 72°C for 60 s) using 0.125 units/sample of *Taq* polymerase (Promega) and one forward primer and one reverse primer from Jackson Laboratory protocol (https://www.jax.org/Protocol?stockNumber=013148&protocolID=22392): forward primer 5'-GCGGTCTGGCAGTAAAAACTATC-3'; reverse primer 5'-GTGAAACAGCATTGCTGTCACTT-3'. Primers amplify within the *Cre* transgene, with a ~120-bp product.

Floxed Lcmt-1: 35 cycles of PCR (95°C for 30 s; 54°C for 30 s; 72°C for 60 s) using 0.125 units/sample of *Taq* polymerase (Promega) and one forward primer and one reverse primer: forward primer 5'-GGGCATAGTAGTTTGCTCTTGTGA-3'; reverse primer 5'-ATAAGAAAGTCTGGTGAAGCTGGC-3'. Primers amplify the downstream *loxP* site (after LCMT-1 exon 3), outside of the *loxP* site. In the wild-type sequence, the product will be 121-bp, but with the 34-bp *loxP* sequence present, the product will be155-bp.

YFP: 35 cycles of PCR (94°C for 60 s; 55°C for 60 s; 72°C for 60 s) using 0.125 units/sample of *Taq* polymerase (Promega), 5% DMSO, and one forward primer and one reverse primer: forward primer 5'-TGAACTTGTGGCCGTTTACG-3'; reverse primer 5'-TCTGAGTGGCAAAGGACCTTAG-3'.

Brain lysate preparation: Brains to be processed for western blot analysis were dissected out without the brain stem, Dounce-homogenized in brain lysis buffer (50 mM Tris-HCl pH 7.4, 150 mM NaCl, 1 mM EDTA, 50 mM sodium fluoride, 0.04 trypsin inhibitor units/ml aprotinin, 10 µM phenylarsine oxide, 1 mM sodium orthovanadate, 100 nM okadaic acid, 1% Nonidet P-40, and 1 mM phenylmethylsulfonyl fluoride) proportional to mass (10 µl per mg of brain tissue) and cleared

via centrifugation for 10 minutes at 13,000 x g. When processing E12.5 brains, embryo heads were transversely cut from the mouth in order to get a complete but not pure representation of the brain.

SDS-PAGE: SDS-PAGE gels were run using a 5% stacking gel and 10% running gel (distilled water, acrylamide, Tris-HCl, SDS, ammonium persulfate, tetramethylethylenediamine) with Bio-Rad Precision Markers. Proteins were then transferred onto nitrocellulose membranes (GVS Life Sciences).

Immunoblotting: Western blots were performed using the following antibodies: anti-LCMT-1 (clone 4A4, 1:3000, Upstate Cell Signaling Solutions, Cat# 05-849), anti-actin (clone C11, 1:2000, Santa Cruz Biotechnologies, Cat# sc-1615), anti-unmethylated PP2A (clone 4b7, 0.5 µg/ml, Santa Cruz Biotechnologies Cat# sc-13601 or EMD Millipore Cat# 05-577), anti-PP2A B55 B subunit: $\alpha>\beta=\delta>\gamma$ (clone 2G9, 1:2000, EMD Millipore, Cat# 05-592), anti-phospho-tau at S262/S356 (clone 12E8, 1:4000, Elan Pharmaceuticals, San Francisco, CA, USA), anti-Tau-1 (1:5000, Millipore, Cat# MAB3420), anti-total 3R tau (1:10,000, gift from Bradley T. Hyman, Harvard Department of Neurology), anti-phospho-CRMP2 at T514 (1:4000, Cell Signaling Technology, Cat# 9397), and anti-CRMP2 (clone 1B1, 1:4000, Santa Cruz Biotechnologies, Cat# sc-101348). Blots were incubated with primary antibodies overnight at 4°C, washed in tris-buffered saline-Tween (TBST), and incubated with Horseradish peroxidase-conjugated secondary antibodies for 1 hour at room temperature. Blots were imaged with a Biorad Fluor S-Max Chemilumimager, which measures band intensities via a super-cooled CCD camera providing linear data >4.8 orders of magnitude. Quantitation was done with Quantity One Software (Bio-Rad). Data presented as a percentage or fold-change relative to control were analyzed in each experiment by first averaging all control values, dividing each experimental (KO, cKO, or Het) value by the average control value, and then taking averages and standard deviations of these ratios from all experiments.

Methylation Assay: PP2A C subunit methylation levels were determined using a previously established protocol [Yu et al., 2001]. Briefly, one aliquot of each lysate was treated for 5 minutes at 4°C with NaOH to completely demethylate PP2A C subunit, followed by neutralization, while another aliquot of equal volume was treated with preneutralized buffer. These samples were analyzed by SDS-PAGE and unmethylated PP2A C subunit levels were detected by immunoblotting with 4b7 anti-unmethylated C subunit antibody. Base-treated lysate 4b7 signal represents 100% unmethylated C subunit, whereas untreated lysate 4b7 signal represents the endogenous level of unmethylated C subunit. Percent methylation was calculated as $100\% - (100\% * \frac{untreated\ lysate\ 4b7\ level}{base-treated\ lysate\ 4b7\ level})$. In some experiments, 4b7 band signals were first normalized to actin for each lane (this was done for cKO experiments but not global KO experiments).

Tau Enrichment: All tau blots were performed on lysates processed with the added tau enrichment step of boiling cleared lysates at 95°C for 5 minutes before being cleared again (also 13,000 x g for 10 minutes at 4°C).

Primary neuronal hippocampal culture: Pregnant dams were euthanized with conscious or unconscious (using isoflurane) cervical dislocation at embryonic day E15.5 and embryo brains were dissected out in Hanks' Balanced Salt solution. One or both hippocampi were isolated and transferred to tubes with minimal carryover of buffer. Hippocampi were manually cut up with small scissors, and then cells were dissociated in 0.25% trypsin with 1 mM EDTA for 15 minutes, agitating every 5 minutes. Digestion was stopped using 1 ml 20% fetal calf serum (FCS) in DMEM, and cells were washed 3 times with hippocampal culture medium (Neurobasal (Invitrogen, Cat# 21103049) with B27, Glutamax, and Penicillin/Streptomycin) by centrifugation at 2000 x g for 1 min at 4°C. Cells were then resuspended in hippocampal culture medium and

plated on 12mm-diameter circle cover glasses, no. 1.5 (Fisher, Cat#1254581), pre-treated overnight with poly-D-lysine (1 mg/ml, Sigma) in 0.1 M borate buffer pH 8.5. Cells were grown for 4 days, with a media change (half replaced) on the second day. Cover glasses were washed in PBS, fixed in 4% paraformaldehyde (PFA) for 15 minutes, and then washed with PBS for 5 minutes followed by 50 mM NH4Cl for 15 minutes to block the PFA. Cells were permeabilized with 0.1% Triton X-100 for 10 minutes, with washes in PBS before and after. Then, cells were blocked with 3% bovine serum albumin (BSA) in PBS with 10% horse serum for one hour, before incubating with primary antibodies overnight (1:200 mouse Tau-1 antibody (Millipore, Cat# MAB3420) and 1:200 rabbit MAP2 antibody (Millipore, Cat# MAB5622) in 3% BSA/PBS, 4°C), washing in PBS, and incubating in secondary antibody for 1 hour (1:200 goat anti-mouse DyLight 594 conjugated (Bethyl, Cat# A90-51D4) and 1:200 goat anti-rabbit DyLight 488 conjugated (Bethyl, Cat# A120-201D2) in 3% BSA/PBS, room temperature). Finally, cover glasses were washed, excess buffer removed, and mounted with Fluoromount G with DAPI (Electron Microscopy Sciences, Cat# 17984-24).

Phenotypic and Behavioral Analysis: Qualitative analysis of cKO newborn mice was conducted to assess the impact of conditional LCMT-1 knockout on normal function and to investigate cause of death. Newborns were checked frequently after birth while minimizing disturbance to them and their mothers. The environment was kept dark until mothers were gently separated from pups for brief periods of analysis. Frequent observation, approximately every 3 hours during the day, enabled accurate estimates of cKO time of death, if occurring during the day. However, time of birth was rarely known, because pregnant mice usually give birth during the night. Nevertheless, the approximate lifespan of 4 cKO pups are known with a margin of error of +/- 5 hours, one of which is known with a +/- 1-hour margin of error. No death was counted from litters in which all

pups died. The above 4 cKO pups, along with one other with longer survival but a wider margin of error, were used to create a viability curve with times of death plotted as midpoints of the time ranges of death.

Besides general observation of newborns for abnormality, visual inspection for milk spots as well as tests for the presence of the suckling response were attempted based on the possibility of the neuronal cKO causing an inability to feed. Milk spots in normal pups are oblong, yellowish-white spots on the mid left abdomen that are visible during the first few days as pups suckle milk from their mother. They can vary in size, with the spots at their largest right after a meal, but they are always visible once a pup has fed at least once. The suckling response was tested by using a cannula-like object to physically stimulate the lips of pups and watching for rhythmic opening and closing of their mouths in response, as performed in another study [Xiang et al., 1996]. When at least one other pup in the litter exhibited this normal phenotype (indicating that the mother is supporting the pups), pups that did not have a milk spot were marked on their belly with a permanent marker.

These potentially abnormal mouse pups were further observed for differences in movement and stability. The main assay that was used was a stability assessment that involved scruffing pups gently and placing them vertically onto a flat sheet of paper. This was repeated 3 times, and if the pup failed to remain upright for more than 3 seconds during all trials, it was deemed unstable. Similar to abnormal milk spot designations, this was only applicable if at least one pup in the litter was stable since entire litters could be affected by poor maternal care.

These analyses were performed at every observational time point to track for any trends or changes. In subsequent data analysis, cKO and non-cKO mice were each divided into pups that always lacked a milk spot or pups had a milk spot at least once. Similarly, analysis for stability

was done, taking stability status at the last observational time point. If, for example, a pup started off stable but got progressively weaker, it was deemed unstable, and if a pup started off unstable but improved, it was deemed stable.

Quantitative PCR: P0 pup brains were isolated, excluding brain stem, and homogenized manually in PBS. A representative portion was pipetted out for digestion overnight and DNA extraction as described previously. Using a NanoDrop 2000 machine to assess DNA concentrations, DNA was diluted to a final concentration of 1.6 ng/µl per sample, a concentration determined to be ideal for accurate amplification. qPCR was then done using SYBR™ Select Master Mix (Applied Biosystems, Cat# 4472908) with two sets of primers. The first primer pair detects the deleted LCMT-1 allele. One primer anneals on either side of the loxP—LCMT-1 exon 3—loxP sequence, which is too long to be amplified in the undeleted condition but will be amplified after Cre excision. The second primer pair detects the undeleted allele. One primer anneals outside the floxed sequence, and one primer anneals inside partially on exon 3 but also partially on a loxP sequence. The latter primer will therefore not bind and allow for amplification of wild-type DNA or LCMT-1 exon 3-deleted DNA. The number of cycles needed to reach threshold of detection (threshold cycle; Ct) was recorded for each sample and for controls, with the difference in Ct values (ΔCt) between the undeleted and deleted conditions (deleted – undeleted) indicating the extent of deletion. The percentage of genomic DNA with exon 3 excised was calculated with the formula $100\% * \frac{2^{\Delta Ct}}{2^{\Delta Ct}+1}$. Primer sets were designed to produce approximately equal sized products and they worked with similar efficiency because the average Ct for the fl/fl undeleted condition approximately matched the average Ct for the cKO deleted condition, given % of cells deleted was eventually calculated to be quite high (~90%). Primers: Deleted condition forward primer 5'-GTCGAGAAGTTCCTATTCCGAAGT-3'; deleted condition reverse primer 5'-

ATAAGAAAGTCTGGTGAAGCTGGC-3'; product when undeleted is 900+ bp (too long to be amplified with the cycle chosen) for both the wild type and floxed condition; product when deleted is 154-bp. Undeleted condition forward primer 5'-GCGCAACGCAATTAATGATAACT-3' (last 6 nt recognize the first 6 nt of the loxP sequence (downstream of LCMT-1 exon 3)); undeleted condition reverse primer 5'-CACAGCACATACAGTACACAGGGT-3'. 159-bp product generated in floxed and undeleted condition, no product generated otherwise.

Weighing: P0 pups were weighed first for total body weight before they were euthanized, their brains were dissected out excluding brain stems, dabbed with a Kimwipe to remove excess liquid, and then the brains were weighed in a microfuge tube.

Cryosectioning: P0 pups, with or without the Thy1-YFP transgene, were euthanized and then their brains were dissected out including brain stem, and excess liquid removed. Then the brains were fixed in 4% PFA at 4°C for 6 hours for YFP imaging, or up to 24 hours for brains used solely for cresyl violet staining. After fixation, PFA was removed and brains were submerged in 30% sucrose in 0.1 M phosphate buffer at 4°C, storing them as such until use. At the time of use, brains were taken out, excess liquid removed, and flash frozen with dry ice-cooled 2-methylbutane in optimum cutting temperature (OCT) compound (Tissue-Tek) using Biopsy Cryomolds (Tissue-Tek), storing them as such at -80°C until further use. Brains were then sliced coronally at 20 µm thickness using a Leica CM1860 Cryostat and transferred to Superfrost Plus microscope slides (Fisher). A slice was taken every 160 µm, with adjacent sections taken for some experiments for cresyl violet staining. Slides were kept cold and air dried before further processing.

YFP brain slice processing: Sections from Thy1-YFP-expressing mice were stained with 2 µg/ml Hoechst in PBS for 7 minutes before washing off with distilled water, air drying, and cover slips were applied using Cytoseal XYL mounting media (Richard-Allan Scientific, Cat# 8312-4).

Cresyl violet staining: Sections were stained in cresyl violet (0.02% filtered cresyl violet in sodium acetate buffer (0.12 M sodium acetate, 0.05 M glacial acetic acid)) for 45 minutes. Sections were then rinsed quickly in distilled water, differentiated quickly with 95% ethanol + 0.04% glacial acetic acid, washed in 100% ethanol, washed in xylene, dried, and mounted with Cytoseal XYL (Richard-Allan Scientific, Cat# 8312-4).

Fluorescence imaging: Hippocampal cells or YFP sections were imaged using an Olympus IX81 phase/fluorescence microscope in conjunction with Slidebook Microscope Analysis software (Intelligent Imaging, Inc.). For YFP sections, hippocampi were imaged at 10x, while retrosplenial cortex areas were imaged at 40x with oil immersion. Calibration was done using a 0.01 mm calibration slide / stage micrometer.

Light microscopy: Cresyl violet-stained sections were photographed with a Nikon Digital Sight DS-Fi1 camera mounted on an Olympus IX81 phase/fluorescence microscope using Nikon Elements D software. Calibration was done using a 0.01 mm calibration slide / stage micrometer.

Quantitation of neuronal morphology: To measure neurite lengths, images from Slidebook were exported as Tiff images—red (Tau-1, axons) and green (MAP2, dendrites and soma) merged. Axons were defined as neurites with the strongest Tau-1 staining extending well beyond where MAP2 staining fades (thus, axons may start out green but become predominantly red extending outwards), while all other neurites were considered dendrites. Axons and dendrites were measured using ImageJ—the segmented line tool was used to trace each neurite from its attachment point at the soma to the end point, followed by a measurement of the length in pixels. Branches were measured separately and added to the total value for each neurite. All neurite lengths for axons and dendrites were averaged for each experiment (not for each neuron). Number of neurites per neuron was averaged for each experiment. Branching complexity was calculated per neurite with the

formula $\frac{\#endpoints}{\#attachment\ points}$ and averaged for each experiment. Number of axons was determined

per neuron and number of neurons with 0, 1, and 2+ axons were counted for each experiment. All

values per experiment (3 total for each parameter) were then averaged with standard deviation,

with t-tests done on these values as well.

Quantitation of YFP neurons: For each experiment, sections that had been numbered previously

during slicing were first aligned for the pair of control and cKO by using the locations of the start

(anterior) and end (posterior) of the hippocampus—the slices where the hippocampal pyramidal

cell layers just start to become visible and just stop being visible. Left hippocampi were paired

with left, and right with right, to account for skewed slicing angles. At least 7 pairs were used per

experiment for hippocampal sections, and 3 pairs per experiment for cortex. To count number of YFP-

expressing neurons in an imperfect but consistent and unbiased way, the particle counting function

of ImageJ was used. Fluorescence images were first carefully thresholded to eliminate background

without merging too many YFP+ neurons together, keeping the threshold consistent between each

matched section pair. To mitigate the impact of merged cells, the binary method, watershed, was

used to separate some cells—this is also an ImageJ algorithm that was applied uniformly to all

images. Non-pyramidal cell layer cells (i.e. dentate gyrus) and other debris were removed from the

image. Finally, the number of particles were analyzed after setting the minimum cell size of 6

pixels^2 (determined after measuring the area of the smallest visible neuron that was still

comfortably larger than any non-neuronal background particle still left over). For each experiment,

the data were then analyzed by first summing total cells counted in right hippocampal sections and

in left hippocampal sections (same number and location of sections in cKO and control, as sections

were matched/paired). The ratio of the number of cells in cKO hippocampus relative to control

was then taken for each side of the hippocampus by dividing these sums. Thus, 2 values result for

each experiment, condensed into one weighted average based on the number of right and number of left hippocampal sections represented (often a different number as not all sections were usable). Finally, these 3 values were averaged with standard deviation.

Quantitation of CA layer thickness: In cresyl violet-stained section images, zoomed in on the CA1, CA2, and CA3 pyramidal cell layers at 32x magnification, thickness of CA pyramidal cell layers was measured using the ImageJ straight line function (lines that would have been drawn are shown for the sections displayed in Figure 8A, right panels). Analysis of these values was done in the same way as the YFP neurons, except with 3 separate average values—one for each of CA1, CA2, and CA3. Each was normalized as a percentage of control as before, but CA1 was also shown as absolute lengths in micrometers (Figure 8C).

Statistical Analysis: All statistical analysis was done in Excel as 2-tailed 1- or 2-sample Student's t-tests, homoscedastic or heteroscedastic for 2-sample tests depending on standard deviation comparisons (F-test). $p < 0.05$ was considered significant with one asterisk, and $p < 0.01$ was considered significant with two asterisks.

Results

Global knockout of LCMT-1 results in decreased LCMT-1 protein levels and PP2A C subunit methylation levels in the fetal brain.

Previously, we have shown that *Lcmt-1* knockout results in embryonic lethality by approximately embryonic day E16.5, and that there are defects in a few tissues, including a consistent indentation in the back of embryo heads suggesting the possibility of a brain development defect [Lee et al., 2018]. In that study, whole embryo levels of LCMT-1 protein and PP2A C subunit methylation levels were greatly reduced [Lee et al., 2018]. We have now

specifically analyzed embryo brains of E12.5 global gene trap KO mice by Western Blotting and Figure 1 shows that PP2A protein and methylation are greatly downregulated, as expected. Specifically, LCMT-1 protein is reduced ~50% with loss of one allele or essentially absent in homozygous KO mice (Figure 1B). Of note, one allele of LCMT-1 is sufficient to provide wild-type levels of PP2A C subunit methylation suggesting their may be no effects of haploinsuffiency for LCMT-1.
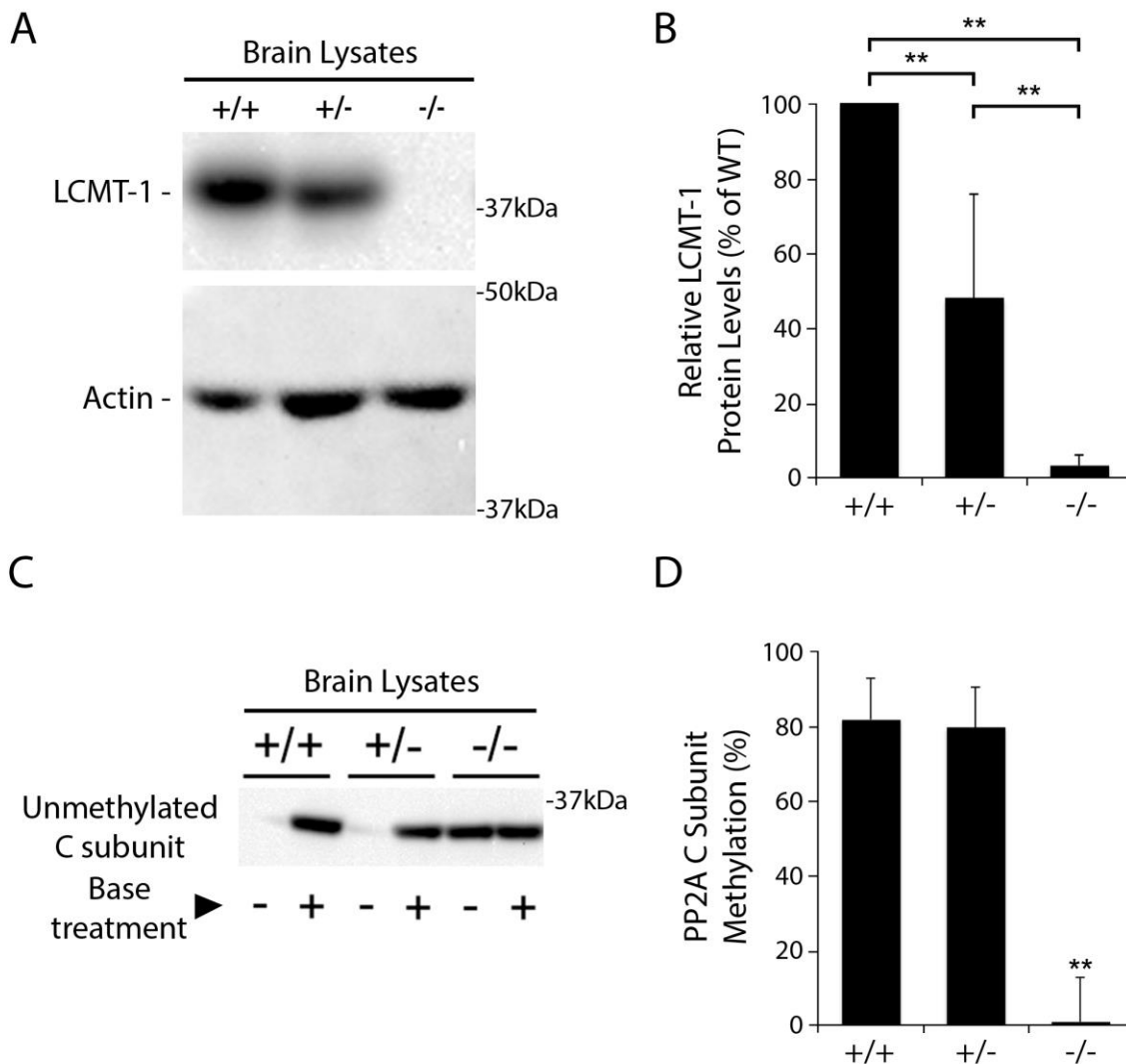
Figure 1. LCMT-1 protein levels and PP2A C subunit methylation levels are greatly reduced in E12.5 LCMT-1 global KO mouse embryo brains. Note: this data is the work of Jocelyn A. Lee. As described in Materials and Methods, mouse embryo brains were lysed and the lysates were analyzed directly by SDS-PAGE and immunoblotting (**A**) or processed for quantitation of PP2A C subunit methylation and then analyzed by SDS-PAGE and immunoblotting (**B**). +/+, LCMT-1$^{+/+}$ (WT), +/-, LCMT-1$^{+/-}$ (Het), -/-, LCMT-1$^{-/-}$ (KO). (**A**) Western blot of lysates showing reduction of LCMT-1 protein in LCMT-1$^{+/-}$ embryo brain and absence in KO brain. (**B**) Results of quantitative analysis of LCMT-1 immunoreactivity from experiments like that shown in (**A**). The data show averages and standard deviations (error bars) of 3 experiments (3 litters: 10 KOs, 9 Hets, and 5 WTs in total). One-sample t-test p values: p<0.001 for WT vs. KO, p<0.001 for WT vs. Het, and p=0.001 for Het vs. KO. (**C**) Western blot showing PP2A C subunit methylation is unaffected in LCMT-1$^{+/-}$ embryo brains but is abolished in KO embryo brains. Immunoreactivity to the antibody 4B7, which detects unmethylated PP2A C subunit, is shown for pairs of lanes loaded with equal amounts of lysate that has either been treated (+) or not treated (-) with base, which demethylates all PP2A C subunit. (**D**) This graph represents the averages and standard deviations (error bars) of PP2A methylation levels from 6 experiments (6 litters: 10 KOs, 11Hets, and 14 WTs in total). Two-sample t-test p-values: p<0.001 for both WT vs. KO and Het vs. KO.

Global knockout of LCMT-1 results in tau hyperphosphorylation at S262 and/or S356 and one or more sites known to inhibit Tau-1 antibody binding (S195, S198, S199, S202).

To investigate the importance of LCMT-1 for regulating the phosphorylation of AD-relevant sites, we analyzed tau phosphorylation in E12.5 global KO embryo brains by performing immunoblotting using 12E8 antibody, which recognizes phosphorylated tau at S262/S356, and Tau-1 antibody, which is inhibited by phosphorylation at S195, S198, S199, or S202 [Szendrei et al., 1993]. Our analysis showed striking hyperphosphorylation at S262/S356 only in KO brains (Figures 2A and 2B)—on average almost 15-fold higher than wild type and heterozygous embryos. Global LCMT-1 KO also caused hyperphosphorylation at one or more of serine residues between 195-202 as indicated by reduced immunoreactivity with the Tau-1 antibody (Figures 2A and 2C). Thus, there is increase in phosphorylation of tau at multiple AD-relevant sites in *Lcmt-1* KO embryo brains.
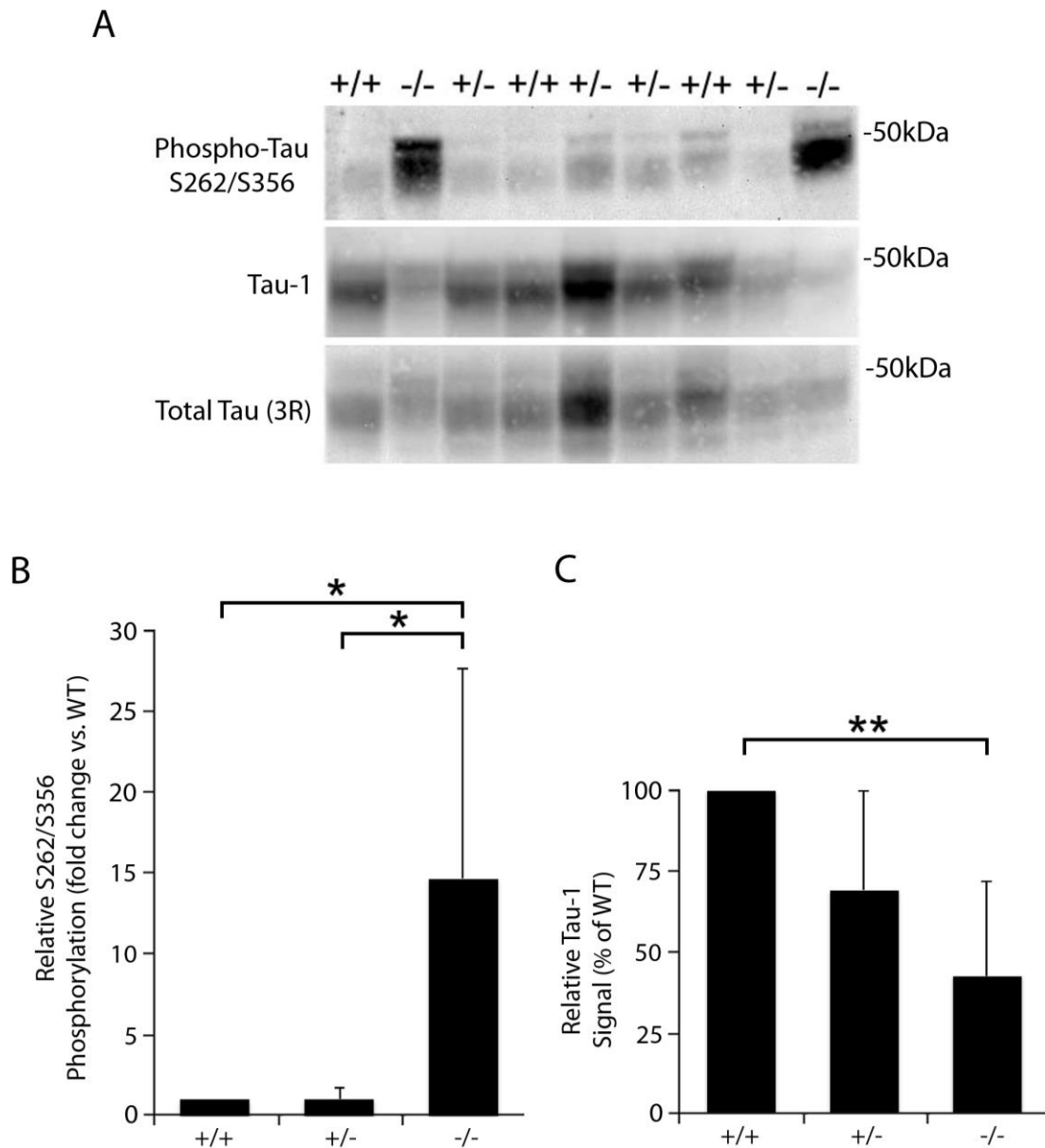
Figure 2. Global KO of LCMT-1 causes hyperphosphorylation of Tau at S262 and/or S356 and at one or more Tau-1 antibody epitope sites (S195, S198, S199, S202) in E12.5 mouse brains. Note: this data is the work of Jocelyn A. Lee. +/+, LCMT-1$^{+/+}$ (WT), +/-, LCMT-1$^{+/-}$ (Het), -/-, LCMT-1$^{-/-}$ (KO). **(A)** Western blot analysis of E12.5 embryo brains from one litter showing Tau is hyperphosphorylated at S262/S356 only in KO brains. Additionally, the blot shows lower immunoreactivity for Tau-1 for KO brains, indicating phosphorylation between tau residues 195-202. **(B)** Quantitative analysis of phosphorylated S262/356 immunoreactivity as normalized to the total tau (3R) level. One- or two-sample t-test p-values: p=0.031 for WT vs. KO, p=0.031 for Het vs. KO. **(C)** Quantitative analysis of Tau-1 immunoreactivity as normalized to the total tau (3R) level. For (B) and (C), the data represent averages ±S.D. for three independent experiments (3 litters: 6 WT, 10 Het, 7 KO). One- or two-sample t-test p-values: p=0.002 for WT vs. KO, p=0.092 for Het vs. KO.

Global knockout of LCMT-1 causes defects in neurite growth and neuronal polarity.

Tau has an important role in regulating microtubule function in neurons and is regulated by phosphorylation. To look for possible defects in global *Lcmt-1* KO neurons, E15.5 hippocampal neurons from global LCMT-1 KO embryos and control littermate embryos were isolated and cultured for 4 days. Immunofluorescence staining with axonal and dendritic markers revealed multiple defects in the growth of KO neurons (Figure 3A-C). First, KO neurite lengths are markedly decreased (Figures 3A and 3B). Quantitative analysis indicates a significant decrease in both axon and dendrite lengths (Figure 3B—top graph). Second, fewer KO neurons display the single-axon morphology characteristic of normal neuronal polarity (Figure 3A and 3C). Compared to control neurons, many more KO neurons either lack an axon or have multiple axons (Figure 3C). In contrast, there is no change in total numbers of neurites per neuron or number of branches per neurite in KO neurons (Figure 3B—middle and bottom graphs). Thus, LCMT-1 is important for neurite growth and neuron polarity.
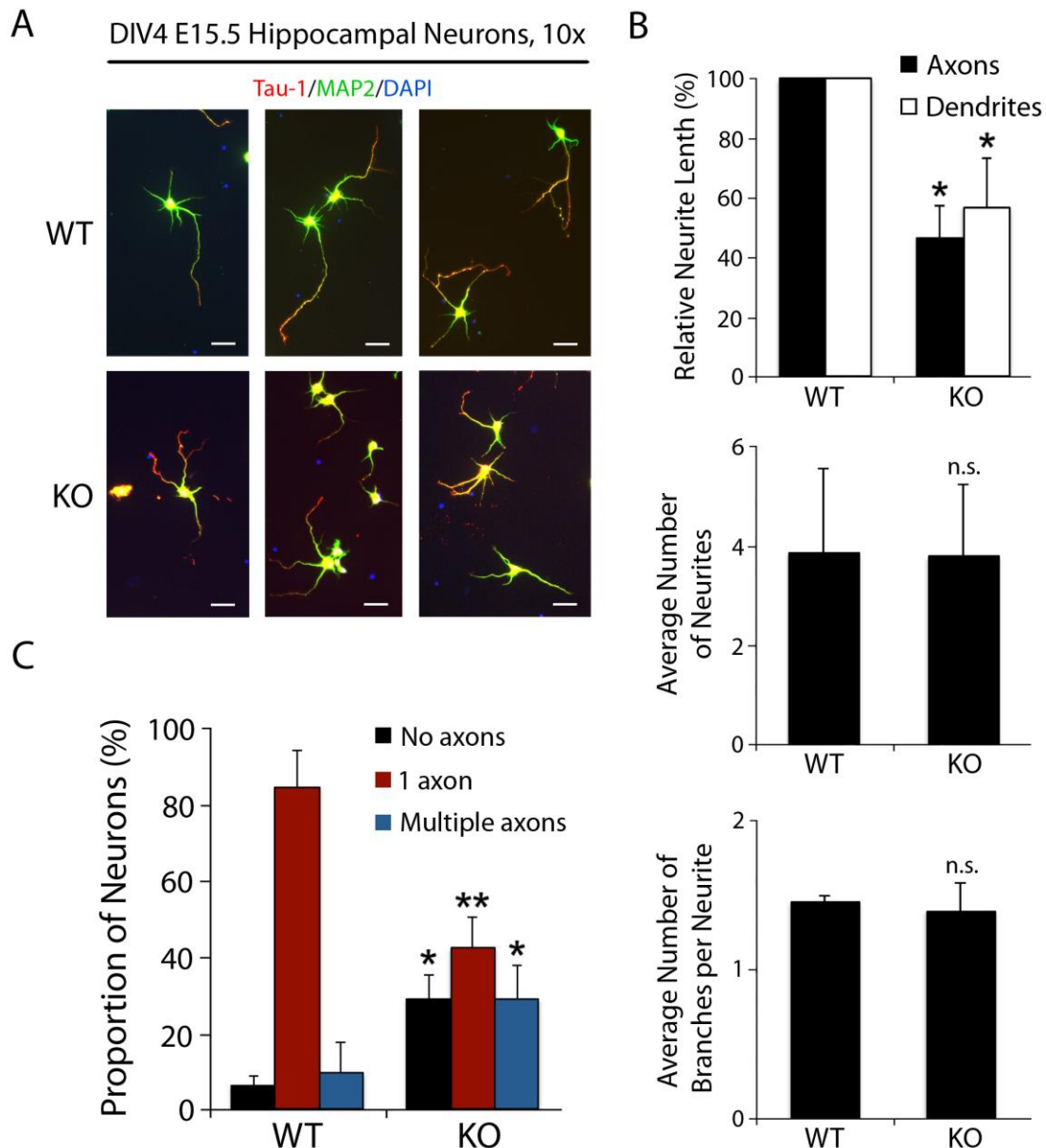
Figure 3. Cultured E15.5 hippocampal neurons display shorter neurites and abnormal numbers of axons. (A) Fluorescence images of hippocampal neurons from WT and KO E15.5 embryos cultured 4 days in vitro (DIV4) and stained for Tau-1 (red; axonal marker), MAP2 (green; dendrite marker), and DAPI (blue; nuclei). Scale bars = 50 μm. **(B)** (Top) Mean length of axons and dendrites in neurons from KO mice as a percentage of the lengths in WT controls. One-sample t-tests yielded p=0.013 for axon length and p=0.046 for dendrite length. (Middle) Mean number of neurites in neurons from WT and KO mice. (Bottom) Mean number of branches per neuron from WT and KO mice. **(C)** Mean numbers (+SD) of neurons with 0, 1, or 2+ axons in cultures from WT and KO mice. Error bars represent standard deviation. Cells studied were from 3 separate litters (3 WT and 5 KO mice). At least 20 neurons per genotype were selected per experiment, with 64 WT and 75 KO neurons analyzed in total. Two-sample Student's t-tests yielded p=0.014 for 0 axons, p=0.005 for 1 axon, and p=0.047 for 2+ axons.

LCMT-1 neuronal-conditional knockout is perinatally lethal, likely due at least in part to an inability to feed.

The global LCMT-1 KO is embryonically lethal by E16.5, with defects in multiple tissues [Lee et al., 2018], but it is unclear what role the neuronal abnormalities we have found in global KO embryos play in this lethality, if any, and what role LCMT-1 plays in the nervous system overall. Thus, a conditional knockout (cKO) of LCMT-1 was generated using the Cre/*loxP* system described in Figure S1 with the *nestin-Cre* mouse line, which is a Cre that expresses broadly in both the central and peripheral nervous system, including neurons and glial cells. In this new mouse model, LCMT-1 floxed exon 3 is deleted in the presence of Cre in nestin-expressing cells, resulting in a change in reading frame after exon 2, a premature stop codon, and only a small, enzymatically inactive fragment of LCMT-1 being expressed.

We developed PCR and qPCR methods for analyzing mice from this colony. Representative PCR products for Cre using published primers and for the floxed LCMT-1 allele using primers described in Materials and Methods are shown in Figure 4. While these PCR products indicate the genotype of pups, they are performed with tail biopsies and give no indication of deletion efficiency. The efficiency of LCMT-1 exon 3 deletion in brain was determined by a qPCR approach outlined in Materials and Methods that allows quantitation of percent deletion of floxed *Lcmt-1* alleles. qPCR analysis of LCMT-1 exon 3 deletion in P0 pup brains revealed that about 90% of floxed exon 3 copies are deleted in both cKO (NesCre$^{+/cre}$ LCMT-1 $^{flox/flox}$) and heterozygous (NesCre$^{+/cre}$ LCMT-1 $^{+/flox}$) mice (Figure 4B), which would translate to about 90% of cells in the brain with exon 3 deletion for heterozygous *Lcmt-1* cKO mice. Since the same result was calculated for cKO mice, it is likely that ~90% of cells in cKO brains have LCMT-1 knocked out. This is assuming that every cell that expresses Cre has both floxed copies excised, but the

percentage of cells with homozygous LCMT-1 exon 3 deletion could be between 80-90% if some

cells only have one copy deleted. LCMT-1 protein levels are correspondingly (~85%) decreased

in homozygous cKO brains, while heterozygous pups have half this decrease (Figure 4C and 4D).
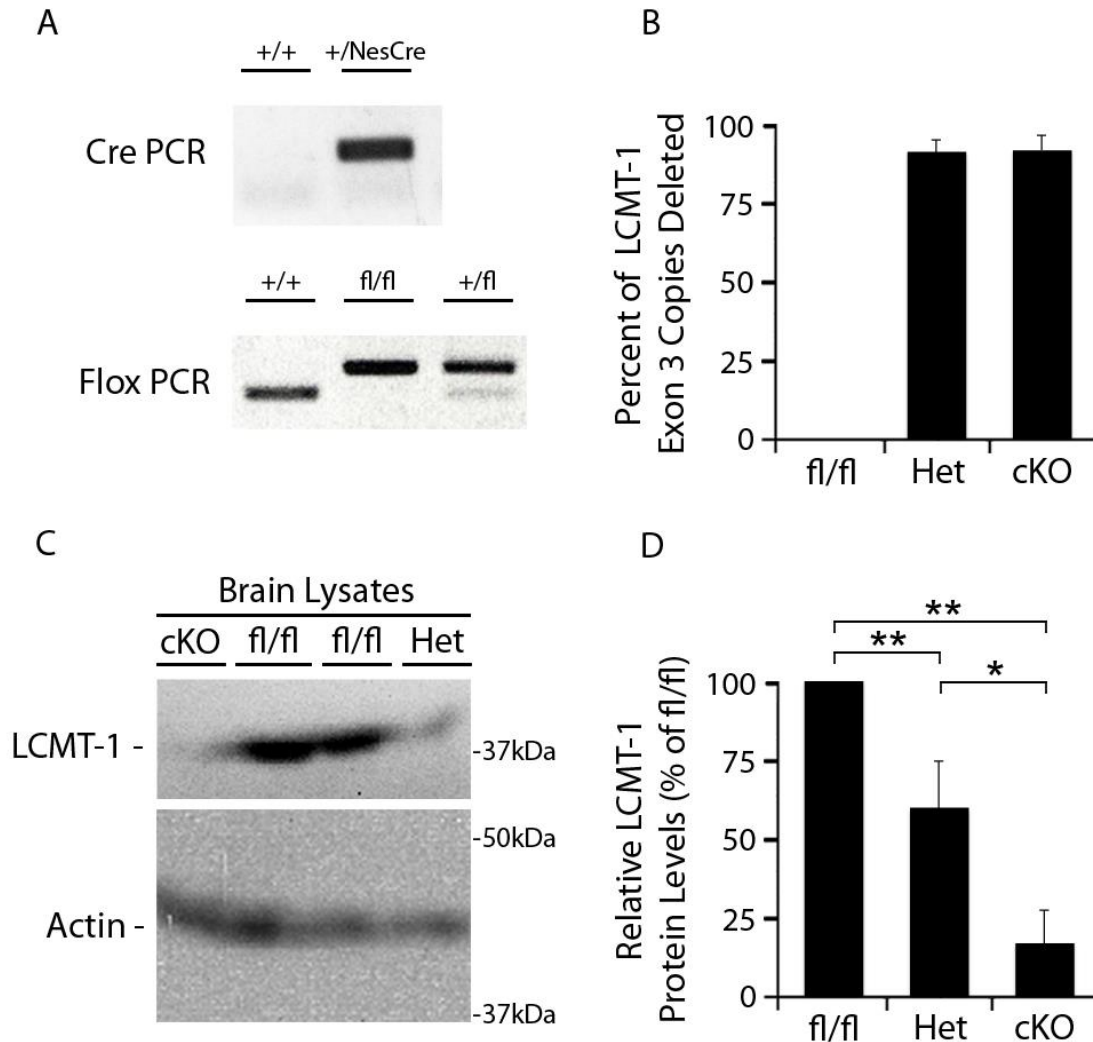
Figure 4. Nestin-Cre mediated cKO of LCMT-1 results in efficient deletion of LCMT-1 exon 3 in P0 pup brains. (A) Shown are agarose gel electrophoresis images of representative genotyping PCR products detecting the presence of Cre (primers designed within the transgene) or Flox (primers designed on either side of one *loxP* sequence so the presence of a floxed LCMT-1 allele makes the PCR product larger). **(B)** Results from qPCR analysis of the extent of knockout in brain tissue is depicted. About 90% of brain cells excise the floxed exon 3 of LCMT-1. P0 brains from 3 experiments (3 litters: 3 cKO, 2 Hets, 2 fl/fls) are represented. Error bar for Het was ±range but for cKO was ± S.D. **(C)** SDS-PAGE and Western Blotting analysis shows that LCMT-1 protein is reduced in Het mice (one copy deleted) and greatly reduced in cKO mice. **(D)** Results of quantitation of LCMT-1 immunoreactivity from immunoblots like the one shown in panel C after normalization to actin as a loading control. The data are representative of 3 experiments (3 litters: 6 cKOs, 3 Hets, and 5 fl/fls in total). cKO, NesCre[+/cre] LCMT-1 [flox/flox]; Het, NesCre[+/cre] LCMT-1 [+/flox]; and fl/fl, NesCre^{+/+} LCMT-1 [flox/flox]. One- or two-sample t-test p-values: $p<0.001$ for fl/fl vs. cKO and fl/fl vs. Het, and $p=0.021$ for Het vs. cKO.

Loss of LCMT-1 in the homozygous cKO translates into dramatically reduced PP2A C subunit methylation levels but the loss of a single allele has no effect on C subunit methylation (Figure 5A and 5B). Correspondingly, there is a moderate decrease in B regulatory subunit levels in cKO pup brains, but no decrease in heterozygous cKO pup brains (Figure 5C and 5D). These results reflect previous data from whole embryos of global LCMT-1 KO mice—LCMT-1 is the sole PP2A methyltransferase, and its loss causes resultant decreases in association of methylation-dependent B subunits (such as the ones blotted for in Figure 5), likely due to higher rates of degradation for these B subunits when not in complex with the A and C subunits [Lee & Pallas, 2018]. Finally, it is important to note that the presence of the Cre itself, as controlled for by heterozygous individuals, does not affect PP2A C subunit methylation or PP2A BAC complex formation.
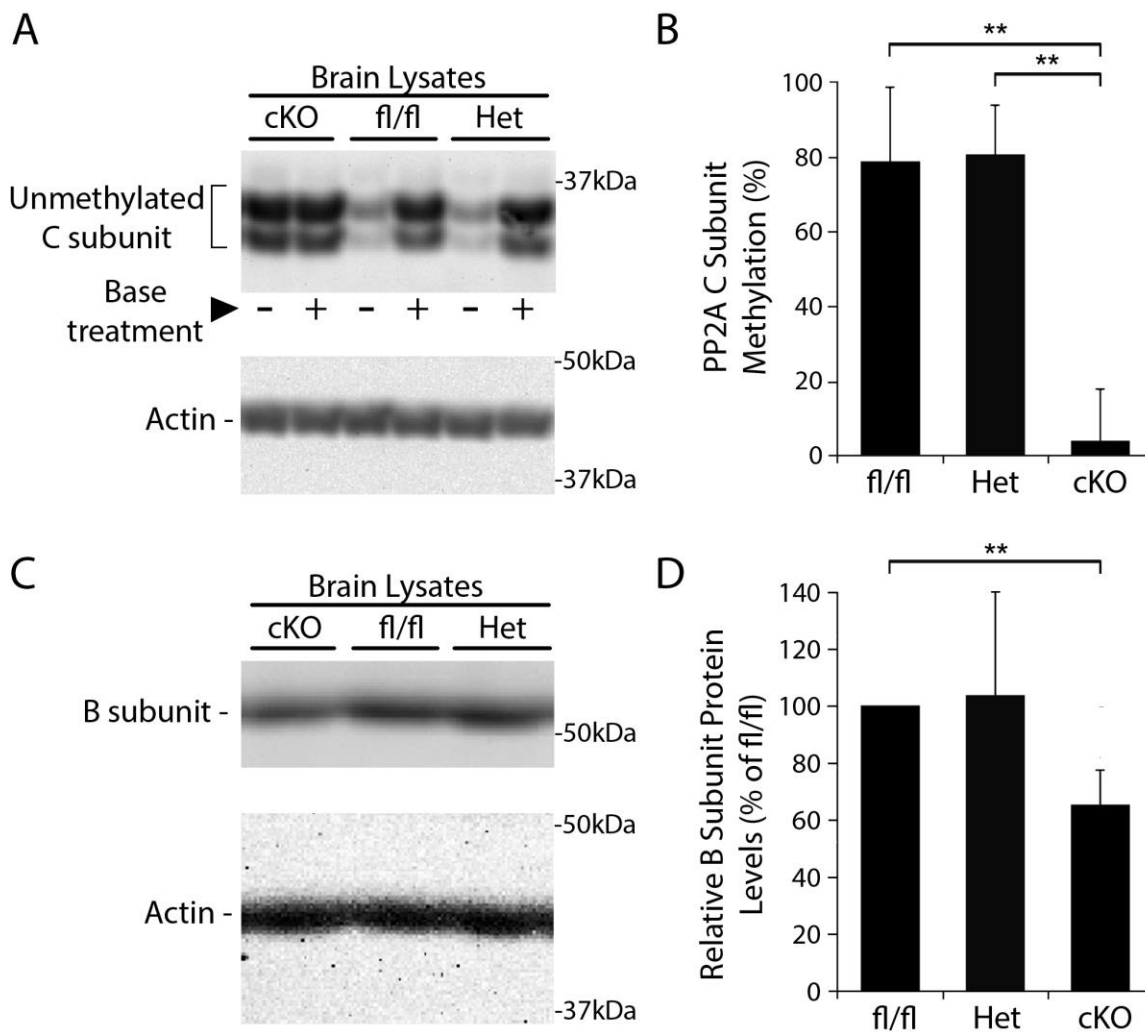
Figure 5. LCMT-1 cKO P0 pup brains have significantly reduced PP2A C subunit methylation and B subunit levels. (A) PP2A C subunit methylation is greatly decreased in cKO mice. Note that PP2A C subunit is known to sometimes run as a doublet as seen here and this does not result from degradation [Hwang et al., 2016]. **(B)** Quantification of PP2A C subunit methylation from 4 experiments (4 litters: 9 cKOs, 7 Hets, and 5 fl/fls in total). Two-sample t-test p-values: p<0.001 for both cKO vs. fl/fl and cKO vs. Het. **(C)** Methylation-dependent B subunits are reduced in cKO pups. **(D)** Quantitation of B subunit immunoreactivity (normalized to actin) shows that loss of LCMT-1 in the vast majority of cKO P0 pup brain cells causes ~35% reduction in B55 levels. The data are representative of 4 experiments (4 litters: 7 cKOs, 5 Hets, and 6 fl/fls in total). cKO, NesCre[+/cre] LCMT-1 [flox/flox]; Het, NesCre[+/cre] LCMT-1 [+/flox]; and fl/fl; NesCre^{+/+} LCMT-1 [flox/flox]. One-sample t-test p-values: p<0.001 for cKO vs fl/fl, p=0.098 for cKO vs. Het.

Next, to investigate the highly penetrant perinatal death phenotype of LCMT-1 cKO mice, observational analysis was undertaken. cKO pups are born alive and were, for the most part, phenotypically and behaviorally normal. However, they have a marked decrease in what appears to be their feeding ability, as a great majority of cKO pups do not develop a milk spot, a visible collection of milk that pups normally suckle from their mothers and store in their stomach (Figure 6A and 6B). To determine if this defect might be due to the absence of suckling ability, we assayed suckling ability by gently stimulating the lips of pups and watching for a rhythmic opening and closing of their jaws in response. A previous study tested in this manner and found deficits in suckling for certain genotypes that also did not have milk spots [Xiang et al., 1996]. For LCMT-1 cKO mice, we found no clear defects in suckling ability using this test, as many cKO mice responded normally to the test (data not shown).

We also observed that cKO mice tended to grow physically weaker over time, moving less and becoming unstable on their feet, as a stability assay showed (Figure 6C). Presumably, the instability ensued as a result of malnutrition—indeed, 82% of pups deemed unstable did not have a milk spot. Furthermore, all four cKO pups with milk spots were considered stable during the time that they had the milk spot. Three of the four were stable throughout observation until the last observational time point, and the fourth eventually became unstable after losing its milk spot. Importantly, this pup was stable while it still had a milk spot (although the milk spot was shrinking), while at the same time point another littermate cKO who had never had a milk spot was already unstable. Lastly, out of 20 total cKO pups without a milk spot, only two were stable. Because the lack or loss of a milk spot thus seems to precede the development of instability, it also makes sense that more cKO pups were deemed stable (~35%, Figure 6D) than had a milk spot (~20%, Figure 6C) in our analysis. Many of the stable cKO pups (mostly without milk spots) likely

would have become unstable if given additional observational time before they died. Importantly, to rule out any litter-wide effects, such as neglectful mothers, no litters were included in these analyses that did not have at least one pup develop a milk spot and have at least one pup stay stable.

Determining time of death after birth could be helpful in determining cause of death. Time of death was estimated for cKO pups where at least one littermate survived 48h after birth. 100% of heterozygote or wild-type pups from 15 litters survived 48h, while no cKO pups out of 9 total survived that long. Based on five cKO pups with known time of birth and/or known time of death within two hours of certainty and survival time known within +/- 5 hours margin of error, cKO pups died on average 22±8h after birth. Figure 6D shows a survival graph for these five pups.
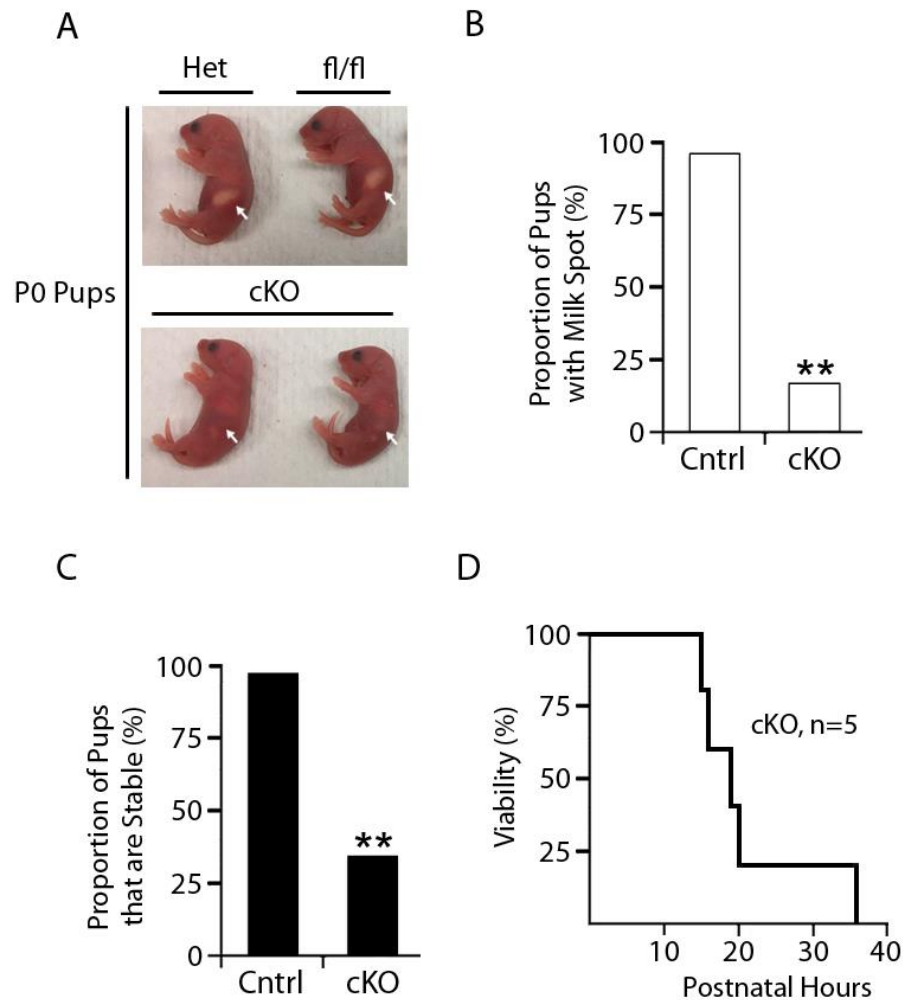
Figure 6. LCMT-1 conditional knockouts are perinatally lethal and exhibit certain distinctive phenotypes. (A) cKO pups lack milk spots. Representative P0 pups from the same litter, genotyped. White arrows indicate the location of the milk spot, whether present or absent/faint. **(B)** cKO pups most often do not develop milk spots. Quantification of the proportion of pups with no milk spot from 15 litters, 25 cKO and 80 control total. $p < 0.001$ for a 2-sample z-test for proportion. **(C)** cKO pups often become unstable. The test for instability involves not being able to stand upright for more than 3 seconds in all of 3 trials (see method section for full description). This was measured at the last time point checked before death of cKO pups in 15 litters, 26 cKO and 83 control pups. $p < 0.001$ for a 2-sample z-test for proportion. cKO, NesCre$^{+/cre}$ LCMT-1$^{flox/flox}$; Het, NesCre$^{+/cre}$ LCMT-1$^{+/flox}$; fl/fl, LCMT-1$^{flox/flox}$; Cntrl, Het or fl/fl. **(D)** Most cKO pups die between about 15-20 hours after birth. Approximate cKO viability curve is displayed, taken from 5 cKO pups with a known birth time and/or known death time within 2 hours of certainty, such that survival time is known in a 10-hour maximum range. The graph represents the midpoints of these time ranges. An exception is the 36-hour death time point, which could have survived anywhere from 27-45 hours.

Global *Lcmt-1* KO mouse embyros typically showed a small but significant reduction in size (Lee et al., 2018). To determine if Nes-Cre directed loss of LCMT-1 had similar effects, we analyzed *Lcmt-1* cKO P0 pups for both brain and body weights. The results shown in Figure 7 indicate that LCMT-1 loss caused a significant decrease of ~10% in both brain and overall body weight. The Nes-Cre transgene itself, as controlled for by heterozygous individuals, seemed to have a small, but not significant negative impact on weight. In 2 of the 8 litters analyzed, there was virtually no difference in both brain and body weight between cKO and controls, with one litter within 1% point of difference for both and one litter actually higher in both weights (data not shown). Thus, the 10% reduction overall in these weights for the eight litters reflect a variable such as time between birth and analysis.
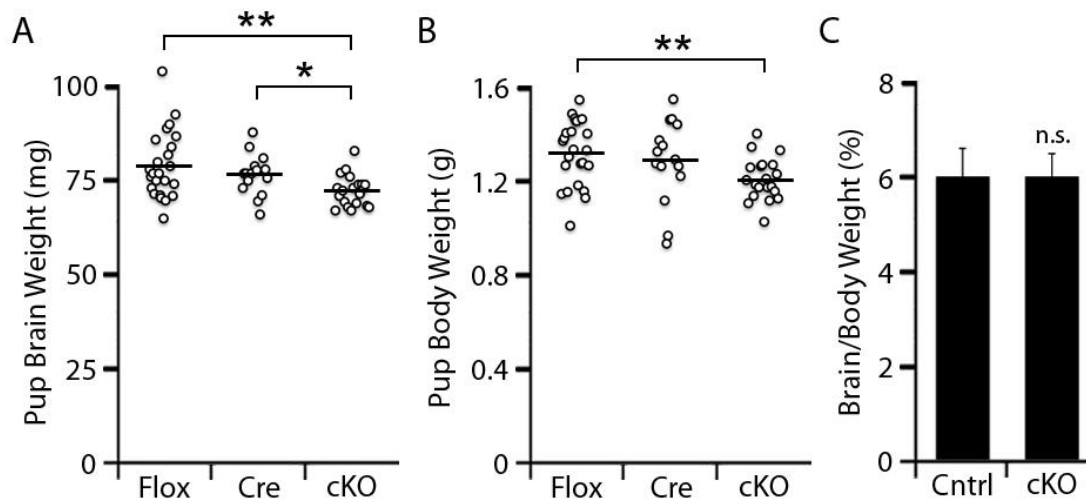
Figure 7. *Lcmt-1* **conditional knockouts have lighter brain weights, but also weigh less overall. (A, B)** *Lcmt-1* cKO mouse brains and body weights are reduced. Depicted are column scatter distributions of pup brain weights, excluding brain stem, and body weights. Brains were dabbed dry prior to weighing. Averages are noted as horizontal bars. 8 litters were used—24 Flox, 15 Cre, and 20 cKO total. Two-sample t-test p-values: *Brain:* 0.002 for Flox vs. cKO and 0.018 for Cre vs. cKO. *Body:* 0.003 for Flox vs. cKO, 0.128 for Cre vs. cKO. **(C)** Lighter brain weight in cKO mice corresponds to lighter weight overall. Brain weight as a percent of body weight for controls and cKO mice is depicted. Flox, NesCre$^{+/+}$ LCMT-1$^{+/flox}$ or NesCre$^{+/+}$ LCMT-1$^{flox/flox}$; Cre, NesCre$^{+/cre}$ LCMT-1$^{+/flox}$ or NesCre$^{+/cre}$ LCMT-1$^{+/+}$; cKO, NesCre$^{+/cre}$ LCMT-1$^{flox/flox}$; Cntrl, Flox or Cre (non-cKO).

LCMT-1 conditional knockout induces hyperphosphorylation of tau.

One possible cause of death would be altered phosphorylation of a protein(s) in the nervous system critical for proper development and function of the brain. Tau is a known substrate of PP2A and is important for regulation of microtubule function in neurons during their differentiation. To probe for tau phosphorylation abnormalities in cKO pup brains, Western blots were performed on P0 cKO pup brains and control brains with the 12E8 and Tau-1 antibodies. For 12E8, the striking difference in phosphorylation seen in Figure 2 between global *Lcmt-1* KO and control embryos was not seen in *Lcmt-1* cKO mice (Figures 8A and 8B). Instead, we observed high immunoreactivity to 12E8 across all genotypes. However, there is an increase in the amount and phosphorylation of an unknown tau isoform marked by * in Figure 8A. This tau isoform is of ~4 kDa lower molecular weight than the lightest known major tau isoform, 3R/0N, which is the predominant isoform at this stage [McMillan et al., 2008].

An important question is whether the phosphorylation of the * isoform has increased in *Lcmt-1* cKO mice. Since there was no detectable signal of this isoform in control pup brains probed with total Tau antibody, we could not simply compare the ratio of phosphorylated * isoform to total * isoform. Thus, we instead compared the ratio of 12E8-detected phosphorylation to total protein levels for the 3R/0N isoform, the 3R/1N, and the * isoform within each *Lcmt-1* cKO lane. This ratio was found to be the highest by a significant margin for the * isoform (Figure 8C). Nevertheless, there is no way to know for sure if this isoform is truly hyperphosphorylated in cKO mice compared to controls or if this isoform is more highly phosphorylated even in the control pup brains. It is clear, however, that the amount of this isoform increases in *Lcmt-1* cKO brains (Figure 8A).
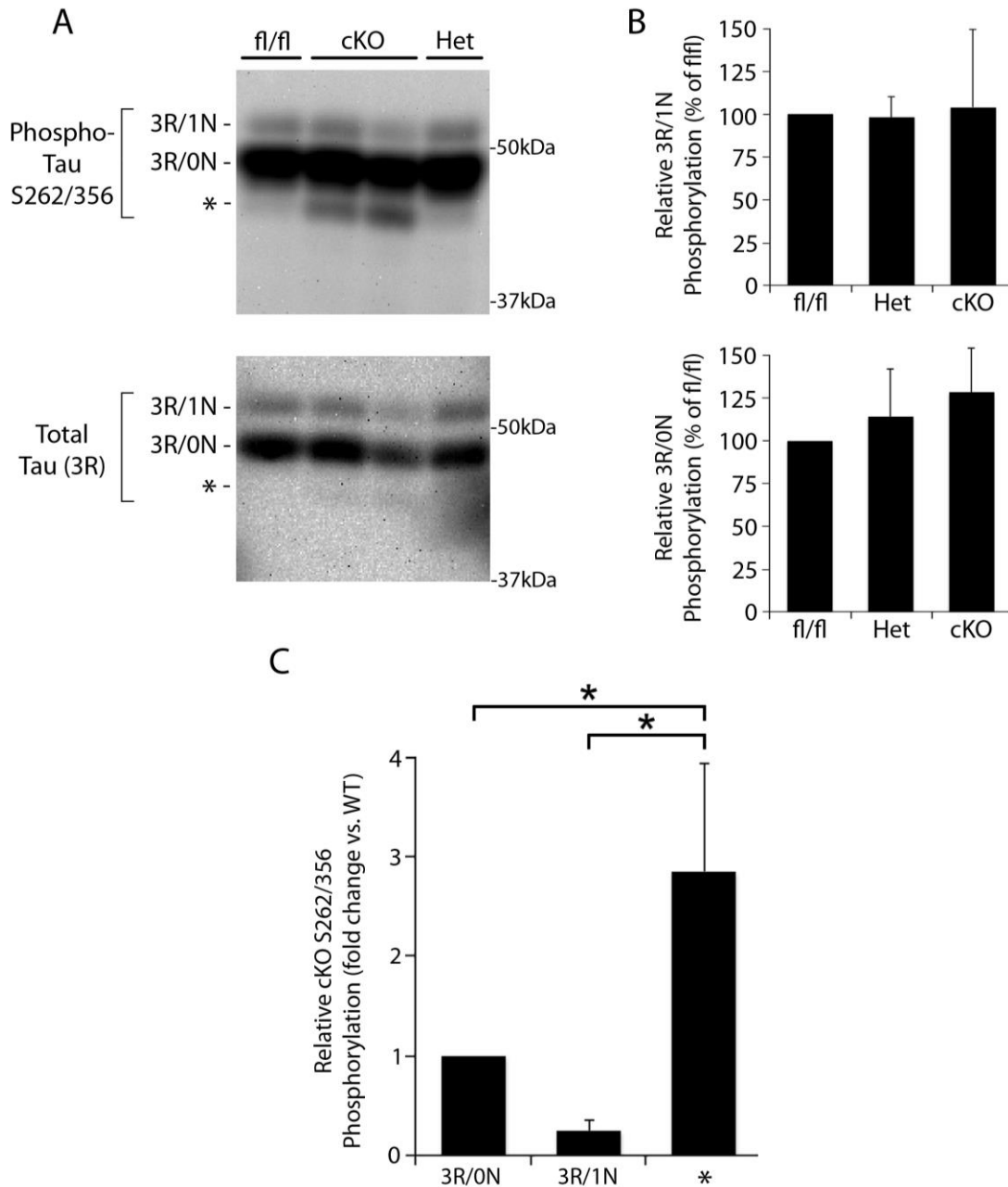
Figure 8. The amount and potentially phosphorylation level at S262 and/or S356 of an unknown isoform of Tau is increased in the brains of P0 *Lcmt-1* cKO mouse pups. (A) Western blotting shows that an unknown tau isoform (*) is increased in protein level and may be hyperphosphorylated at S262/S356 in *Lcmt-1* cKO mice. **(B)** Shown are the results from experiments like that shown in panel A of quantitation of the phosphorylation immunoreactivity to 12E8 of 3R/1N and 3R/0N and normalization to the corresponding isoform's total level. **(C)** Comparison of the ratios of phosphorylation level normalized to total protein for each isoform in the *Lcmt-1* cKO lanes. For ease of comparison, the value for 3R/0N was set to 1 and the others were graphed relative to that. cKO, NesCre[+/cre] LCMT-1 [flox/flox]; Het, NesCre[+/cre] LCMT-1 [+/flox]; and fl/fl, NesCre^{+/+} LCMT-1 [flox/flox]. All data are representative of 3 experiments (3 litters: 4 fl/fl, 4 Het, 4 cKO). One-sample t-test p-values: p=0.042 for phosphorylation ratio between 3R/0N and *, and p=0.017 for 3R/1N vs. *.

Probing with the Tau-1 antibody on the other hand did reveal tau hyperphosphorylation in *Lcmt-1* cKO pup brains because Tau-1 signal is down in cKO brains (Figure 9). This result indicates that loss of LCMT-1 causes hyperphosphorylation at one or more of the sites of the Tau-1 epitope where phosphorylation has been reported to block Tau-1 antibody binding (S195, S198, S199, and S202) [Szendrei et al., 1993].
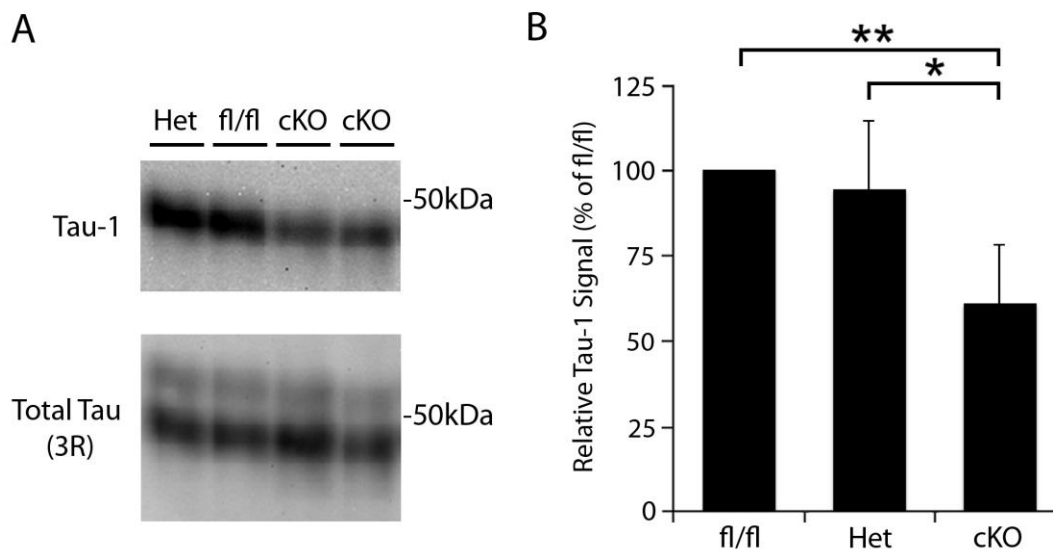
Figure 9. Loss of LCMT-1 in *Lcmt-1* cKO mouse P0 pup brains causes tau hyperphosphorylation. **(A)** Western blotting shows *Lcmt-1* cKO decreases Tau-1 binding, indicating increased phosphorylation at one or more of the Tau-1 epitope phosphorylation sites: S195, S198, S199, or S202 [Szendrei et al., 1993]. **(B)** Quantitation and normalization of the Tau-1 immunoreactivity to the total tau (3R) immunoreactivity. cKO, NesCre[+/cre] LCMT-1 [flox/flox]; Het, NesCre[+/cre] LCMT-1 [+/flox]; fl/fl, NesCre^{+/+} LCMT-1 [flox/flox]. The data are representative of 3 experiments (3 litters: 4 fl/fl, 3 Het, 5 cKO). One-sample t-test p-values: p=0.007 for fl/fl vs. cKO, p=0.0459 for Het vs. cKO.

Hippocampal neurons are decreased in *Lcmt-1* cKO P0 mouse pups.

To begin to probe potential structural defects in the brain that could help explain the lethality of *Lcmt-1* cKO pups, we mated the conditional knockout model with a neuronally-YFP-expressing model to allow for visualization of neurons by YFP fluorescence. P0 mouse brains were fixed, sliced, mounted, and imaged for YFP fluorescence, with a set of adjacent sections stained with cresyl violet. After computer analysis with ImageJ, we found that numbers of YFP-expressing neurons are decreased in cKO P0 pups in the cornu ammonis (CA) pyramidal cell layers of the hippocampus (Figure 10A). While YFP expresses only in a subset of neurons, YFP neuron numbers are known to correlate with total neuron number [Feng et al., 2000]. Thus, these data suggest that loss of LCMT-1 reduces the number of hippocampal neurons. This decrease is not seen in all areas of the brain, as shown by the fact that we found YFP+ neuron counts to be similar between the cKO and control P0 pups in a cortical area, the retrosplenial cortex (Figure 10A, bottom panels). Furthermore, preliminary analysis of overall neuronal cell density in ~10 brain slices from cKO and control pup brains stained with cresyl violet showed no significant difference (data not shown), lending further support to our finding of a region-specific rather than a widespread defect. Importantly, these effects are not simply due to expression of *nestin-Cre*, because in 2 of 3 experiments the controls had NesCre$^{+/cre}$.
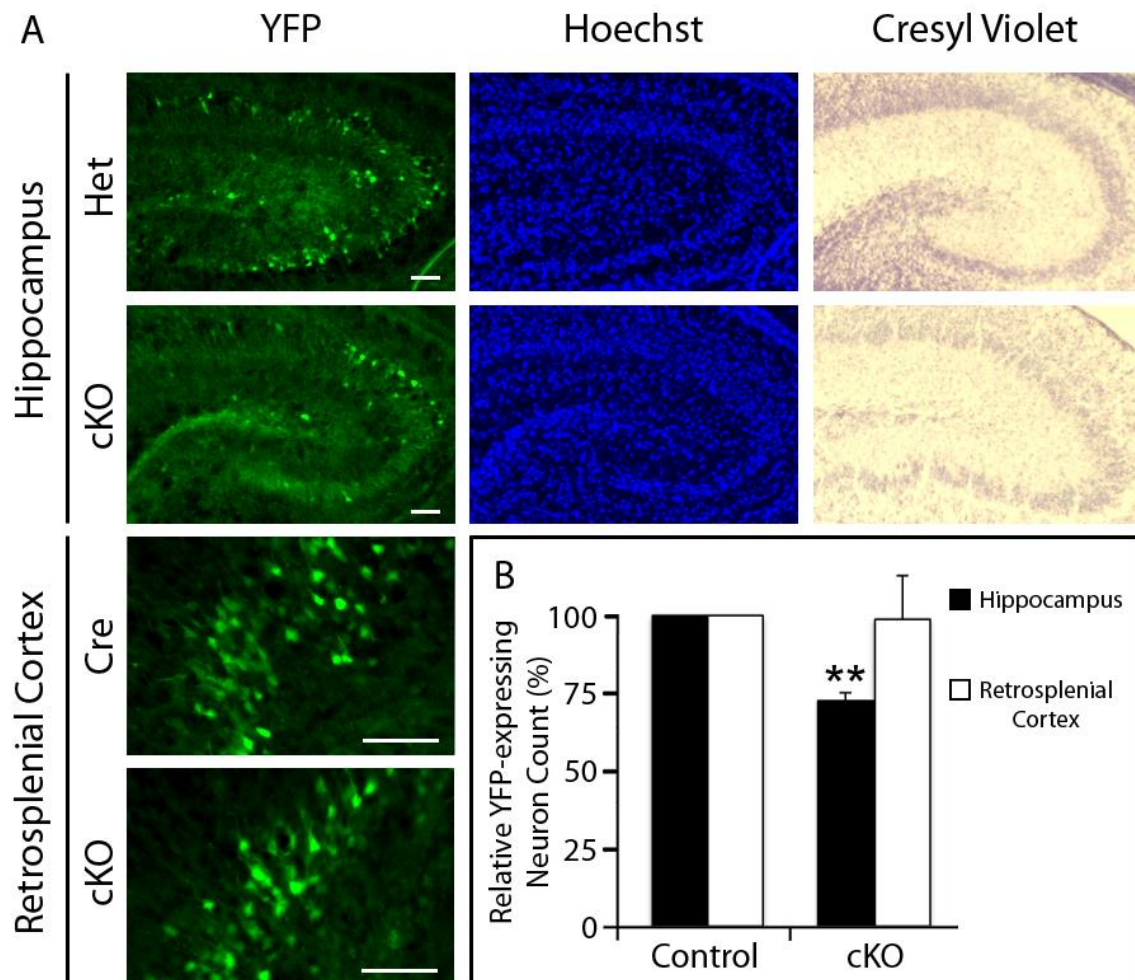
Figure 10. *Lcmt-1* **cKO pups have a selective reduction of hippocampal neurons in the cornu ammonis (CA) pyramidal cell layers.** (**A**) The number of YFP+ neurons in the hippocampus is decreased in cKO mice. Shown are YFP and Hoechst-stain fluorescence images and cresyl violet-stained bright-field images of representative hippocampal sections taken from brain slices in one experimental pair (Het vs. cKO, littermates). Also shown are YFP images of sections of a representative control area (retrosplenial cortex; Cre vs. cKO). YFP and Hoechst images were taken of the same hippocampal slice, and cresyl violet images were taken from the same hippocampi but in the immediately adjacent slice. (**B**) Quantification of the relative number of YFP-expressing neurons present in control vs. cKO P0 pups in both hippocampus (just the CA pyramidal cell layers, not the dentate gyrus) and cortex. At least 7 pairs of sections were used per experiment for hippocampal sections, and 3 pairs per experiment for cortex. Scale bars represent 50 µm. cKO, NesCre$^{+/cre}$ LCMT-1$^{flox/flox}$; Het, NesCre$^{+/cre}$ LCMT-1$^{+/flox}$; Cre, NesCre$^{+/cre}$ LCMT-1$^{+/+}$. 3 experiments (each comparing littermate pairs) of P0 mice—cKO vs. LCMT-1$^{+/flox}$, cKO vs. Het, and cKO vs. Cre—are represented. One-sample t-test yielded p=0.0026 between cKO and control for hippocampus.

The finding of a decrease in hippocampal neuron number in *Lcmt-1* cKO pups by the neuronal YFP approach is also supported by finding of thinner cornu ammonis (CA) pyramidal cell layers in *Lcmt-1* cKO P0 pups as visualized by cresyl violet staining in an adjacent brain slice (Figure 10A, right). Quantitative analysis on cresyl violet slices (Figure 11A) of the layer thicknesses of each of CA1, CA2, and CA3 reveals a significant decrease in CA1 layer thickness in cKO mice (Figures 11B), and decreased thicknesses for CA2 and CA3, although not statistically significant (p=0.326 and p=0.491), potentially due to lower resolution of these two layers because they are thinner. All 3 experiments in this analysis had a *nestin-Cre*-containing control, so the presence of *nestin-Cre* itself did not influence these results.
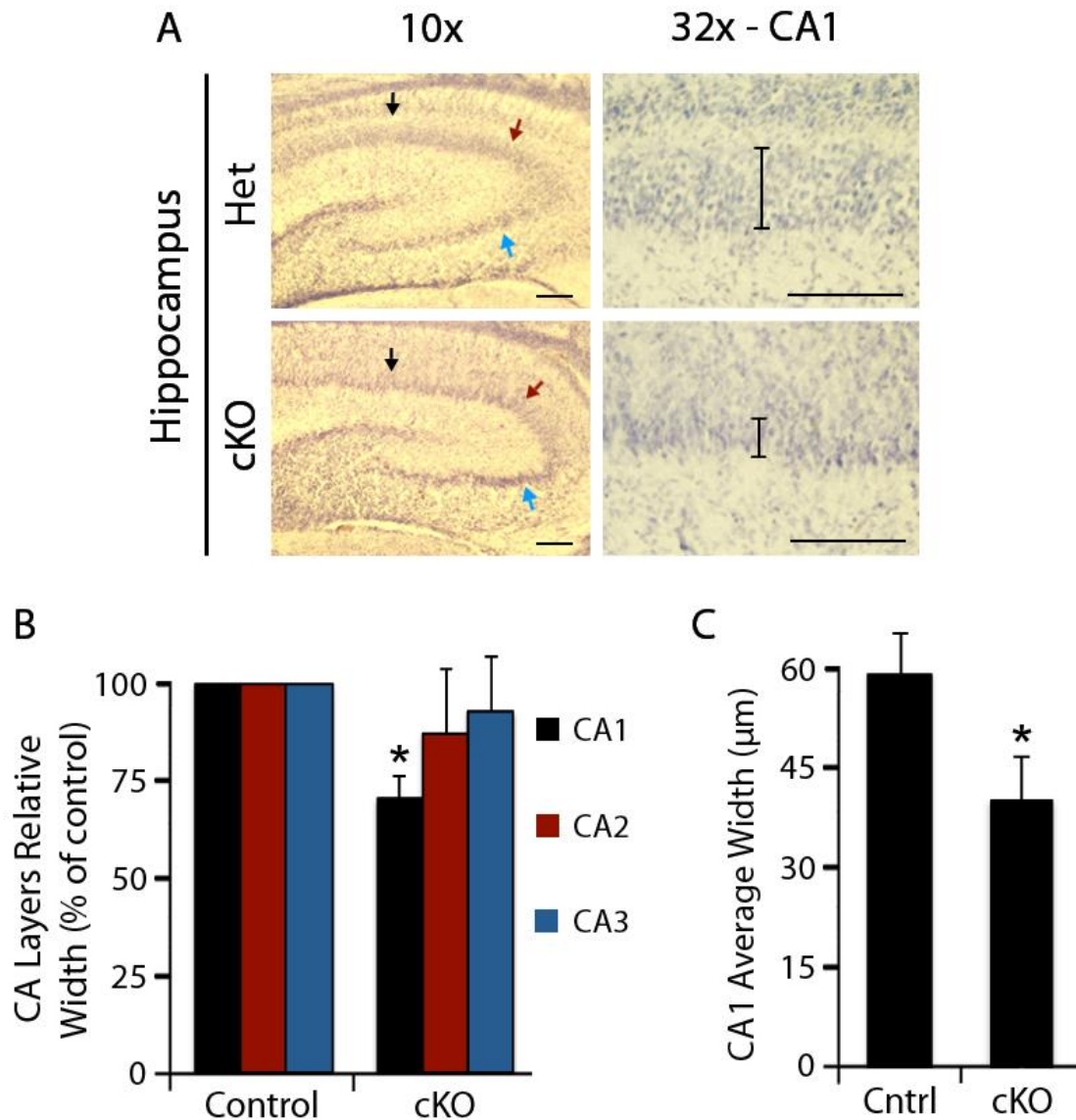
Figure 11. *Lcmt-1* **cKO P0 pups have thinner cornu ammonis (CA) pyramidal cell layers. (A)** CA cell layer width, particularly CA1, is decreased in cKO mice. Representative cresyl violet-stained hippocampal sections taken from brain slices from one experimental pair (Het vs. cKO, littermates) are shown. The 10x view (left) additionally displays arrows representing the approximate location used across all images to measure pyramidal cell layer thickness at CA1 (black), CA2 (red), and CA3 (blue). The 32x view (right) of a magnified CA1 area additionally includes bars representing the way in which cell layer thicknesses were measured using the ImageJ straight line function. **(B)** Results from quantification of the relative thickness of cell layers by CA1, CA2, and CA3. At least 6 section pairs were used per experiment. One-sample t-tests yielded p=0.013 for CA1, and p=0.326 and p=0.491 for CA2 and CA3, respectively. **(C)** Quantification of the CA1 cell layer thickness of control vs. cKO by absolute width in micrometers, as converted from pixels using a microscope stage micrometer. Scale bars represent 0.1 mm. cKO, NesCre[+/cre] LCMT-1[flox/flox]; Het, NesCre[+/cre] LCMT-1[+/flox]; 3 experiments of paired P0 pup littermates—cKO vs. Het, cKO vs. Het, and cKO vs. Cre—are represented. Two-sample t-test yielded p=0.021.

Discussion

In this study, we have investigated the role of LCMT-1 in the nervous system using a previously published global *Lcmt-1* KO mouse model as well as a novel *Lcmt-1* cKO mouse model. We characterized the new cKO model and found that it efficiently deleted *Lcmt-1* in the nervous system. In addition, using biochemical analyses, explanted neurons, and transgenic neuron-specific YFP expression, we have demonstrated that LCMT-1 loss results in neuronal and biochemical defects, and that LCMT-1 is a necessary component of neuronal development and survival.

Dysregulation of tau phosphorylation upon LCMT-1 loss.

Loss of LCMT-1 in both global *Lcmt-1* KO and the *Lcmt-1* cKO mouse models examined here causes tau hyperphosphorylation, a hallmark of AD and other tauopathies. The most consistent finding was hyperphosphorylation of the Tau-1 antibody epitope. Tau hyperphosphorylation at many sites, including S199 and S202 (Tau-1 epitope sites [Szendrei et al., 1993]), and S262 (and/or the similar site of S356, which is in an analogous sequence in another repeat domain), is correlated with AD [Bertrand et al., 2010]. In addition, Tau-1 immunoreactivity is decreased in AD postmortem brain [Ksiezak-Reding et al., 1988]. Furthermore, the phosphorylation state of S262 has been associated with pretangle neurons (neurons beginning to form NFTs) [Augustinack et al., 2002]. Some studies have thus far only correlated LCMT-1 downregulation with AD [Park et al., 2018]. In contrast, our findings provide direct evidence that LCMT-1 downregulation results in this aberrant state of tau. In addition, our data indicate that this effect can be induced at a very early stage of development.

The difference between the global *Lcmt-1* KO and the *Lcmt-1* cKO mouse models in regard to tau S262/356 phosphorylation was striking. Global loss of LCMT-1 shows a strong induction of hyperphosphorylation on the major tau isoforms while conditional LCMT-1 loss does not. Several explanations are possible. First, the difference may be due to a difference in knockout method. Although both the global and conditional knockout should have similar knockout levels in brain, the global knockout affects many other non-neuronal cell types that may indirectly impact tau phosphorylation in the brain. For example, basic fibroblast growth factor (bFGF) has been found to be elevated in AD brain, and induces an increase in tau phosphorylation ex vivo [Burack & Halpain, 1996]. The difference could also arise because of analysis at different developmental time points—E12.5 for the global knockout and P0 for the conditional. Unfortunately, it is difficult to directly compare the two knockout conditions at the same time point, as *nestin-Cre* does not reach its peak of expression until around E17.5 [Liang et al., 2012], by which point LCMT-1 global KO embryos would already have died [Lee et al., 2018].

The different time point of analysis brings up another possibility that there indeed is a real dampening in the apparent hyperphosphorylation of tau in LCMT-1 knockouts compared to controls. Another tau phosphatase could arise and compensate for downregulated PP2A between E12.5 and P0, but perhaps the more likely possibility is that phosphorylation of tau ramps up in the latter half of gestation, such that the absolute level of phosphorylation by P0 is very high or even saturated. This idea is supported by previous studies that have found significantly higher levels of tau phosphorylation at multiple sites during development, peaking in the first week of postnatal life. For example, using the AT8 antibody, which recognizes important AD-associated tau phosphorylation sites, phosphorylation was detectable at around E18, peaked at P0, and faded by P15 [Burack & Halpain, 1996], with results mirrored in other sites analyzed as well (the 12E8

site was not analyzed by this study). Thus, tau phosphorylation may be dynamically regulated over developmental time.

Neuronal polarity and neurite growth defects in global KO embryo neurons.

Our results clearly indicate abnormal neuronal polarity in neurons explanted from global KO embyros. Neuronal polarity refers to the asymmetric process by which neurites are differentially destined for different fates—development into axons (usually one per neuron) and dendrites. This occurs in a three-phase process which involves the extension of small neurite sprouts, growth of individual sprouts into one rapidly-extending axon and several dendrites, and maturation of neurites into functional forms [Cáceres et al., 2012].

Finding abnormal numbers of axons implies there may be a defect in the second phase of neuronal polarity development—the selection of one and only one neurite to extend and grow rapidly as an axon. The axonal growth cone develops at this stage, followed by the recruitment of several master regulators of cytoskeletal arrangement such as CRMP2 and GSK3β [Cáceres et al., 2012], both of which are targeted by PP2A [Zhu et al., 2010, Lin et al., 2007]. Disruption or overexpression of these cytoskeletal regulators leads to abnormal numbers of axons. For example, CRMP2 is critical for axon differentiation [Fukata et al., 2002] and GSK3β mutants result in axonal inhibition when overactive and multiple-axon formation when inhibited [Jiang et al., 2005]. Taken together, this information could explain the phenotype we observe, because PP2A downregulation through LCMT-1 deletion could, for example, inhibit axon formation in some cells through phosphorylation-dependent inactivation of CRMP2, and promote multiple-axon formation in other cells through a similar inactivation of GSK3β but with the opposite effect. Furthermore, many of these cytoskeletal regulators have been shown to regulate neurite extension as well by mediating

recruitment and incorporation of cytoskeletal elements, and so the downregulation of these proteins could contribute overall to the decreased neurite length we observed in the KO hippocampal cells.

Experiments addressing a possible role for CRMP2 in mediating LCMT-1 effects on neuronal polarity suggest CRMP2 is not involved in LCMT-1 function in neuronal polarity. CRMPs play integral roles in the developing brain by mediating proper cytoskeletal arrangement during neuronal differentiation [Brot et al., 2014], a key process of which is neuronal polarity. CRMPs are primarily regulated through phosphorylation, and two CRMPs have already been found to be regulated by PP2A. However, we have found that CRMP2 phosphorylation is unchanged in cKO mice (Figure S2), suggesting that CRMP2 phosphorylation is not regulated by methylation-dependent PP2A and LCMT-1. Nevertheless, there are other potential players in neuronal polarity that are potential LCMT-1 targets and future work should focus on potential mediators of neuronal polarity that may be regulated by LCMT-1. To this end, we have identified RSK2 and DOCK7, two neuronal proteins that are involved in neurite outgrowth and/or are located at the axonal growth cone, as possible candidates based on finding their phosphorylation levels increased by mass spectrometry upon loss of LCMT-1 in global *Lcmt-1* KO embryos (data not shown).

LCMT-1 may also affect neuronal polarity and neurite growth via its effects on tau phosphorylation. While tau is a component of AD pathogenesis, it is also a cytoskeletal regulator implicated in the process of neuronal polarity and maturation. Our finding that tau is hyperphosphorylated at S262 in LCMT-1 global KO embryos is especially tied into this hypothesis as downregulation of S262 phosphorylation is correlated with longer neurite length [Chen et al., 2014]. Thus, hyperphosphorylation at S262 induced by LCMT-1 loss likely contributes to the

shorter neurite length we observe in explanted, differentiating neurons. S262 is located within the tubulin-binding domain of tau and its phosphorylation state is a main factor in microtubule-binding capacity [Biernat et al., 1993], which likely contributes to its importance in neurite growth. Additionally, dephosphorylation of S262 is correlated with relocation of tau from the cell body to neurites, where it then can associate with tubulin and mediate microtubule formation, which is also dependent on S262 dephosphorylation [Chen et al., 2014]. Thus, tau hyperphosphorylation caused by LCMT-1 loss may contribute to the global KO neuronal growth and differentiation defects.

Appearance of an unknown isoform of tau in *Lcmt-1* cKO P0 mouse brain extracts.

The identity of the unknown isoform found increased in both amount and possibly phosphorylation level remains to be determined. It is not one of the 6 canonical isoforms of tau. Tau undergoes alternative splicing in two regions, the microtubule-binding region and the amino-terminal region, to form either 3-repeat (3R) or 4-repeat (4R) and either 0N (no insert), 1N (1 insert), or 2N (2 inserts) isoforms, giving 6 types of isoforms in total [McMillan et al., 2008]. In mice, the 3R isoforms are predominant in embryonic development, and the 4R isoforms become predominant by adulthood [Pîrşcoveanu et al., 2017]. The 4R isoforms are absent at P0 and start to be expressed by 2 weeks postnatal [Liu & Götz, 2013].

In terms of known non-canonical tau isoforms, our * isoform does not seem to be the right size for isoforms without the microtubule-binding domain [Luo et al., 2004]. Beyond this study, few others have detailed alternative splice variants beyond those that result in the 6 canonical isoforms. Many more have investigated post-translational modifications of tau, such as ubiquitination, glycosylation, glycation, acetylation, nitration, and others. None of these are known to cause a downward shift in band location on SDS-PAGE. The most likely possibility is

truncation, which can occur from the action of different proteases. Examples of proteases known to truncate tau are aminopeptidases, lysosomal proteases like cathepsin, calpain, thrombin, and others [Zhou et al., 2018, Wang et al., 2007]. Perhaps the most extensively studied, however, is cleavage at D421 by caspase 3, which has been implicated in AD pathology [Gamblin et al., 2003]. Of all the possible proteolytic cleavages, the cleavage event at D421 is among the most likely to match the ~4 kDa shift downwards in the * isoform from 3R/0N. PP2A has been shown to target S422 dephosphorylation [Deters et al., 2009], a site that is hyperphosphorylated in AD brain [Augustinack et al., 2002]. Pseudo-phosphorylation at this site shown to inhibit the D421 cleavage [Sandhu et al., 2017]. Thus, PP2A downregulation would be expected to increase phosphorylation at S422 and thus inhibit cleavage by caspase 3, making our * isoform less likely to be this proteolytic product. However, further work should be done to investigate this and other truncated forms of tau.

A region-specific neuronal deficit exists in *Lcmt-1* cKO P0 mouse pup brains.

An important novel finding from our studies is that LCMT-1 is important for generation and/or survival of the proper amount of hippocampal neurons. This conclusion is based on finding a reduction in YFP$^+$ neurons in the hippocampus but not the cortex and on finding a thinning of the CA1 region of the hippocampus in *Lcmt-1* cKO P0 pup brains. The neuronal deficit we have found in hippocampi of *Lcmt-1* cKO mice is important because the hippocampus is a key site of AD pathogenesis. The hippocampus is impacted early in AD onset, along with other particularly vulnerable brain areas, a selective deterioration that matches the phenotype we observe in our cKO mice. It has also been shown that dysfunctional hippocampal neurogenesis in particular is implicated in AD; thus, enhancing neurogenesis may be a therapeutic approach that could boost

neuronal plasticity and memory retention [Mu and Gage, 2011]. Thus, if our *Lcmt-1* cKO hippocampal phenotype is best characterized by a loss of neurogenesis, LCMT-1 may regulate hippocampal neurogenesis and thus may be important in the development of AD.

Although altered phosphorylation of tau might contribute to this phenotype (Figure 10, 11), there is currently minimal evidence for a specific mechanism to explain these selective effects. LCMT-1 and PP2A have been implicated in cell cycle control and prevention of apoptosis [Lee and Pallas, 2007]. While one might expect that enhancement of apoptosis by LCMT-1 reduction might be reflected in more widespread neuronal cell death, it could be that LCMT-1 regulates a key process for survival in only the pyramidal cells of the hippocampus (and potentially other neuronal areas). Selective or preferential apoptosis upon LCMT-1 or PP2A C subunit deletion has been reported for red blood cells vs other blood cells, for example (Lee et al., 2018). PP2Ac has also been shown to be necessary in preventing apoptosis of red blood cell precursors [Lee et al., 2018]. PP2Ac has also been shown to be necessary in preventing apoptosis of red blood cell precursors [Chen et al., 2011]. While no preliminary evidence for apoptosis was found in Hoechst-stained sections in the form of nuclear fragmentation, apoptosis could have occurred at an earlier stage of development and further investigation at various developmental stages using more rigorous apoptosis assays must be done to pursue this line of investigation.

Another possibility that might explain a selective effect is that LCMT-1 deficit in the cKO pups not only occurs in neurons but also in certain glial cells that support them. In this case, a selective hippocampal deficit might be explained by the increased vulnerability of CA pyramidal cells to stressors such as ischemia [Nitatori et al., 1995]. Glial cells that might be involved include astrocytes, which cause decreased neurite outgrowth and survival in culture when they are dysfunctional [Lange et al., 2018].

Perinatal lethality of *Lcmt-1* cKO mice.

While it is clear that LCMT-1 conditional knockouts die perinatally, a full explanation remains to be elucidated. It is likely due at least in part to an inability to feed, as noted by a lack of milk spot development in cKO pups. Importantly, the timeframe of lethality we have established of death averaging ~22 hours after birth closely matches the timeframes established by another study with a similar absent milk spot phenotype [DeChiara et al., 1995]. However, it is unclear whether this is the only reason, as preliminary rescue attempts with intraperitoneal glucose or saline injections have been unsuccessful at extending survival (data not shown).

There are many possibilities as to why pups are unable to feed. Pups may not be able to suckle milk, as another study with a similar phenotype noted [DeChiara et al., 1995]. They may not have an appetite, as regulated by the autonomic nervous system, or may not be able to orient to their mother's nipples properly. The latter could be a motor deficit, although we have noted that cKO pups seem to move normally. Finally, the deficit could be olfactory because during navigation to the nipple, pups follow odor substrates released by the dam [Aïn et al., 2013].

With regards to the differences we have found in weight, it is likely that the primary reason is due to a difference in nutritional intake between cKO and control pups. Both brain and overall body weight are lower in cKO pups on average by the same amount. Thus, the decrease in brain weight is likely not explained by a lower number of cells in the brain, but by a general decrease in weight, which might be caused by the greatly reduced liquid and nutrition intake. This possibility is supported by the fact that, as noted previously, a few litters did not accrue any difference in weights between cKO and control mice. 2 litters in particular were within 2% points for brain weight yet had somewhat lower pup weights for cKO mice, potentially indicating that a difference in pup weight likely appears first, followed by a delay before a difference in brain weight is seen.

Thus, the brains of cKO mice are either stunted in growth compared to control pups or lacking in water weight. Much work needs to be done to investigate the mechanistic explanations for the lethality in cKO mice. Many of the neurological deficits we have noted in global KOs and cKOs may contribute, such as the dysregulated tau phosphorylation or abnormal neuronogenesis. For example, tau hyperphosphorylation could be disrupting neuronal cytoskeletal networks and thus inducing abnormal neuronogenesis, and this in turn could disrupt nervous system development.

Concluding remarks

Importantly, it should be noted that although our attention has been focused on PP2A, LCMT-1 also methylates PP4 and PP6 [Hwang et al., 2016], and regulates stable assembly of PP4 methylation-dependent heterotrimers as it does for PP2A. Thus, any of the effects of LCMT-1 knockout that we have noted could be due to PP4 and/or PP2A downregulation.

Another important note is that *nestin-Cre* expression occurs later in gestation, beginning at around E14.5 and becoming sufficient for widespread recombination by E17.5 [Liang et al., 2012], meaning that the timeline of LCMT-1 knockout in cKO mice differs from that of global KO embryos, where LCMT-1 is dysfunctional from the start of development. The results we find here, and any discrepancies between global KO and cKO mice we have noted, could thus be influenced by the timing and/or pattern (exogenous effects) of expression. If LCMT-1 conditional knockout started earlier in development, we might have seen more severe defects and consequences.

In this study, our findings represent the first developmental-stage *in vivo* manipulation of LCMT-1 neuronally that bolsters data from studies [Park et al., 2016, Park et al., 2018, Vogelsberg-Ragaglia et al., 2001] that only correlate PP2A and LCMT-1 downregulation with neuronal diseases or only study it *in vitro* [Yang et al., 2016, Sontag et al., 2013, Deters et al.,

2009]. However, a recent study showed that overexpression of LCMT-1 in the forebrain of adult mice was found to protect mice from β-amyloid peptide (Aβ)-induced cognitive and electrophysiological impairments, while overexpression of PME-1, the methylesterase that removes methyl groups added by LCMT-1, protected from Aβ-induced effects [Nicholls et al. 2016]. Our approach differs from analysis in adult mice in that it represents a focus towards analysis of LCMT-1 function developmentally, with more indirect analysis of AD-related pathology. However, our results show for the first time that LCMT-1 expression in the nervous system is a necessary component of neuronal development and is required for postnatal survival.

Overall, our work has helped elucidate the role LCMT-1 and PP2A play in the nervous system and its development, and hopefully will spur future research into the mechanisms underlying the action of PP2A in neurons. Altering the Cre driver used for conditional *Lcmt-1* deletion in the nervous system to provide less ubiquitous expression of Cre will likely allow more extensive analyses of the relevance of LCMT-1 function in diseases like AD.

References

1. Wlodarchak N, Xing Y. PP2A as a master regulator of the cell cycle. Crit Rev Biochem Mol Biol. 2016 Jun;51(3):162–84.
2. Vogelsberg-Ragaglia V, Schuck T, Trojanowski JQ, Lee VM. PP2A mRNA expression is quantitatively decreased in Alzheimer's disease hippocampus. Exp Neurol. 2001 Apr;168(2):402–12.
3. Lee JA, Pallas DC. Leucine carboxyl methyltransferase-1 is necessary for normal progression through mitosis in mammalian cells. J Biol Chem. 2007 Oct 19;282(42):30974–84.
4. Hwang J, Lee JA, Pallas DC. Leucine Carboxyl Methyltransferase 1 (LCMT-1) Methylates Protein Phosphatase 4 (PP4) and Protein Phosphatase 6 (PP6) and Differentially Regulates the Stable Formation of Different PP4 Holoenzymes. J Biol Chem. 2016 Sep 30;291(40):21008–19.
5. Lee JA, Wang Z, Sambo D, Bunting KD, Pallas DC. Global loss of leucine carboxyl methyltransferase-1 causes severe defects in fetal liver hematopoiesis. J Biol Chem. 2018 22;293(25):9636–50.

6. Ogris E, Du X, Nelson KC, Mak EK, Yu XX, Lane WS, et al. A protein phosphatase methylesterase (PME-1) is one of several novel proteins stably associating with two inactive mutants of protein phosphatase 2A. J Biol Chem. 1999 May 14;274(20):14382–91.

7. Bernal A, Arranz L. Nestin-expressing progenitor cells: function, identity and therapeutic implications. Cell Mol Life Sci. 2018;75(12):2177–95.

8. Park H-J, Lee K-W, Oh S, Yan R, Zhang J, Beach TG, et al. Protein Phosphatase 2A and Its Methylation Modulating Enzymes LCMT-1 and PME-1 Are Dysregulated in Tauopathies of Progressive Supranuclear Palsy and Alzheimer Disease. J Neuropathol Exp Neurol. 2018 Feb 1;77(2):139–48.

9. Yu XX, Du X, Moreno CS, Green RE, Ogris E, Feng Q, et al. Methylation of the Protein Phosphatase 2A Catalytic Subunit Is Essential for Association of Bα Regulatory Subunit But Not SG2NA, Striatin, or Polyomavirus Middle Tumor Antigen. Mol Biol Cell. 2001 Jan;12(1):185–99.

10. Park H-J, Lee K-W, Park ES, Oh S, Yan R, Zhang J, et al. Dysregulation of protein phosphatase 2A in parkinson disease and dementia with lewy bodies. Ann Clin Transl Neurol. 2016;3(10):769–80.

11. Sontag J-M, Nunbhakdi-Craig V, Sontag E. Leucine carboxyl methyltransferase 1 (LCMT1)-dependent methylation regulates the association of protein phosphatase 2A and Tau protein with plasma membrane microdomains in neuroblastoma cells. J Biol Chem. 2013 Sep 20;288(38):27396–405.

12. Sontag J-M, Nunbhakdi-Craig V, Mitterhuber M, Ogris E, Sontag E. Regulation of protein phosphatase 2A methylation by LCMT1 and PME-1 plays a critical role in differentiation of neuroblastoma cells. J Neurochem. 2010 Dec;115(6):1455–65.

13. Liang H, Hippenmeyer S, Ghashghaei T. A Nestin-cre transgenic mouse is insufficient for recombination in early embryonic neural progenitors. Biol Open. 2012 Dec;1(12):1200-3.

14. Declercq J, Brouwers B, Pruniau VPEG, Stijnen P, Faudeur G de, Tuand K, et al. Metabolic and Behavioural Phenotypes in Nestin-Cre Mice Are Caused by Hypothalamic Expression of Human Growth Hormone. PLOS ONE. 2015 Aug 14;10(8):e0135502.

15. Feng G, Mellor RH, Bernstein M, Keller-Peck C, Nguyen QT, Wallace M, et al. Imaging neuronal subsets in transgenic mice expressing multiple spectral variants of GFP. Neuron. 2000 Oct;28(1):41–51.

16. Biernat J, Gustke N, Drewes G, Mandelkow E-., Mandelkow E. Phosphorylation of Ser262 strongly reduces binding of tau to microtubules: Distinction between PHF-like immunoreactivity and microtubule binding. Neuron. 1993 Jul 1;11(1):153–63.

17. Chen Q, Zhou Z, Zhang L, Xu S, Chen C, Yu Z. The Cellular Distribution and Ser262 Phosphorylation of Tau Protein Are Regulated by BDNF In Vitro. PLoS One [Internet]. 2014 Mar 11;9(3). Available from: https://www.ncbi.nlm.nih.gov/pmc/articles/PMC3950283/

18. Brot S, Smaoune H, Youssef-Issa M, Malleval C, Benetollo C, Besançon R, et al. Collapsin response-mediator protein 5 (CRMP5) phosphorylation at threonine 516 regulates neurite outgrowth inhibition. Eur J Neurosci. 2014 Oct;40(7):3010–20.

19. Pîrşcoveanu DFV, Pirici I, Tudorică V, Bălşeanu TA, Albu VC, Bondari S, et al. Tau protein in neurodegenerative diseases - a review. Rom J Morphol Embryol. 2017;58(4):1141–50.

20. Martin L, Latypova X, Wilson CM, Magnaudeix A, Perrin M-L, Terro F. Tau protein phosphatases in Alzheimer's disease: the leading role of PP2A. Ageing Res Rev. 2013 Jan;12(1):39–49.

21. Yang C, Kuai X, Gao W, Yu J, Wang Q, Li L, et al. Morroniside-Induced PP2A Activation Antagonizes Tau Hyperphosphorylation in a Cellular Model of Neurodegeneration. J Alzheimers Dis. 2016;51(1):33–44.

22. Wang Y, Yang R, Gu J, Yin X, Jin N, Xie S, et al. Cross talk between PI3K-AKT-GSK-3β and PP2A pathways determines tau hyperphosphorylation. Neurobiol Aging. 2015 Jan;36(1):188–200.

23. McMillan P, Korvatska E, Poorkaj P, Evstafjeva Z, Robinson L, Greenup L, et al. Tau isoform regulation is region and cell-specific in mouse brain. J Comp Neurol. 2008 Dec 20;511(6):788–803.

24. Conrad C, Zhu J, Conrad C, Schoenfeld D, Fang Z, Ingelsson M, et al. Single molecule profiling of tau gene expression in Alzheimer's disease. Journal of Neurochemistry. 2007 Nov 1;103(3):1228–36.

25. Liu C, Götz J. Profiling Murine Tau with 0N, 1N and 2N Isoform-Specific Antibodies in Brain and Peripheral Organs Reveals Distinct Subcellular Localization, with the 1N Isoform Being Enriched in the Nucleus. PLoS One. 2013;8(12).

26. Xiang, M., Gan, L., Zhou, L., Klein, W. H., & Nathans, J. (1996). Targeted deletion of the mouse POU domain gene Brn-3a causes selective loss of neurons in the brainstem and trigeminal ganglion, uncoordinated limb movement, and impaired suckling. Proceedings of the National Academy of Sciences, 93(21), 11950-11955.

27. Bertrand J, Plouffe V, Sénéchal P, Leclerc N. The pattern of human tau phosphorylation is the result of priming and feedback events in primary hippocampal neurons. Neuroscience. 2010 Jun 30;168(2):323–34.

28. Augustinack JC, Schneider A, Mandelkow E-M, Hyman BT. Specific tau phosphorylation sites correlate with severity of neuronal cytopathology in Alzheimer's disease. Acta Neuropathol. 2002 Jan;103(1):26–35.

29. Burack MA, Halpain S. Site-specific regulation of Alzheimer-like tau phosphorylation in living neurons. Neuroscience. 1996 May 1;72(1):167–84.

30. Cáceres A, Ye B, Dotti CG. Neuronal polarity: demarcation, growth and commitment. Curr Opin Cell Biol. 2012 Aug;24(4):547–53.

31. Nicholls RE, Sontag J-M, Zhang H, Staniszewski A, Yan S, Kim CY, et al. PP2A methylation controls sensitivity and resistance to β-amyloid–induced cognitive and electrophysiological impairments. Proc Natl Acad Sci U S A. 2016 Mar 22;113(12):3347–52.

32. Zhu L-Q, Zheng H-Y, Peng C-X, Liu D, Li H-L, Wang Q, et al. Protein phosphatase 2A facilitates axonogenesis by dephosphorylating CRMP2. J Neurosci. 2010 Mar 10;30(10):3839–48.

33. Lin C-F, Chen C-L, Chiang C-W, Jan M-S, Huang W-C, Lin Y-S. GSK-3beta acts downstream of PP2A and the PI 3-kinase-Akt pathway, and upstream of caspase-2 in ceramide-induced mitochondrial apoptosis. J Cell Sci. 2007 Aug 15;120(Pt 16):2935–43.

34. Jiang H, Guo W, Liang X, Rao Y. Both the establishment and the maintenance of neuronal polarity require active mechanisms: critical roles of GSK-3beta and its upstream regulators. Cell. 2005 Jan 14;120(1):123–35.

35. Fukata Y, Itoh TJ, Kimura T, Ménager C, Nishimura T, Shiromizu T, et al. CRMP-2 binds to tubulin heterodimers to promote microtubule assembly. Nat Cell Biol. 2002 Aug;4(8):583–91.

36. Burack MA, Halpain S. Site-specific regulation of Alzheimer-like tau phosphorylation in living neurons. Neuroscience. 1996 May 1;72(1):167–84.

37. Luo M, Tse S-W, Memmott J, Andreadis A. Novel isoforms of tau that lack the microtubule-binding domain. Journal of Neurochemistry. 2004;90(2):340–51.

38. Zhou Y, Shi J, Chu D, Hu W, Guan Z, Gong C-X, et al. Relevance of Phosphorylation and Truncation of Tau to the Etiopathogenesis of Alzheimer's Disease. Front Aging Neurosci. 2018;10.

39. Szendrei GI, Lee VM, Otvos L. Recognition of the minimal epitope of monoclonal antibody Tau-1 depends upon the presence of a phosphate group but not its location. J Neurosci Res. 1993 Feb 1;34(2):243–9.

40. Wang YP, Biernat J, Pickhardt M, Mandelkow E, Mandelkow E-M. Stepwise proteolysis liberates tau fragments that nucleate the Alzheimer-like aggregation of full-length tau in a neuronal cell model. Proc Natl Acad Sci U S A. 2007 Jun 12;104(24):10252–7.

41. Gamblin TC, Chen F, Zambrano A, Abraha A, Lagalwar S, Guillozet AL, et al. Caspase cleavage of tau: Linking amyloid and neurofibrillary tangles in Alzheimer's disease. Proc Natl Acad Sci U S A. 2003 Aug 19;100(17):10032–7.

42. Sandhu P, Naeem MM, Lu C, Kumarathasan P, Gomes J, Basak A. Ser422 phosphorylation blocks human Tau cleavage by caspase-3: Biochemical implications to Alzheimer's Disease. Bioorg Med Chem Lett. 2017 01;27(3):642–52.

43. Deters N, Ittner LM, Götz J. Substrate-specific reduction of PP2A activity exaggerates tau pathology. Biochem Biophys Res Commun. 2009 Feb 6;379(2):400–5.

44. Nitatori T, Sato N, Waguri S, Karasawa Y, Araki H, Shibanai K, et al. Delayed neuronal death in the CA1 pyramidal cell layer of the gerbil hippocampus following transient ischemia is apoptosis. J Neurosci. 1995 Feb;15(2):1001–11.

45. Ksiezak-Reding H, Binder LI, Yen SH. Immunochemical and biochemical characterization of tau proteins in normal and Alzheimer's disease brains with Alz 50 and Tau-1. J Biol Chem. 1988 Jun 15;263(17):7948–53.

46. Chen W, Gu P, Jiang X, Ruan H-B, Li C, Gao X. Protein Phosphatase 2A Catalytic Subunit α (PP2Acα) Maintains Survival of Committed Erythroid Cells in Fetal Liver Erythropoiesis through the STAT5 Pathway. Am J Pathol. 2011 May;178(5):2333–43.

47. DeChiara TM, Vejsada R, Poueymirou WT, Acheson A, Suri C, Conover JC, et al. Mice lacking the CNTF receptor, unlike mice lacking CNTF, exhibit profound motor neuron deficits at birth. Cell. 1995 Oct 20;83(2):313–22.

48. Aïn SA, Belin L, Schaal B, Patris B. How does a newly born mouse get to the nipple? odor substrates eliciting first nipple grasping and sucking responses. Developmental Psychobiology. 2013;55(8):888–901.

49. Mu Y, Gage FH. Adult hippocampal neurogenesis and its role in Alzheimer's disease. Mol Neurodegener. 2011 Dec 22;6:85.

50. Lange J, Haslett LJ, Lloyd-Evans E, Pocock JM, Sands MS, Williams BP, et al. Compromised astrocyte function and survival negatively impact neurons in infantile neuronal ceroid lipofuscinosis. Acta Neuropathol Commun. 2018 Aug 8;6.

Supplemental Figures
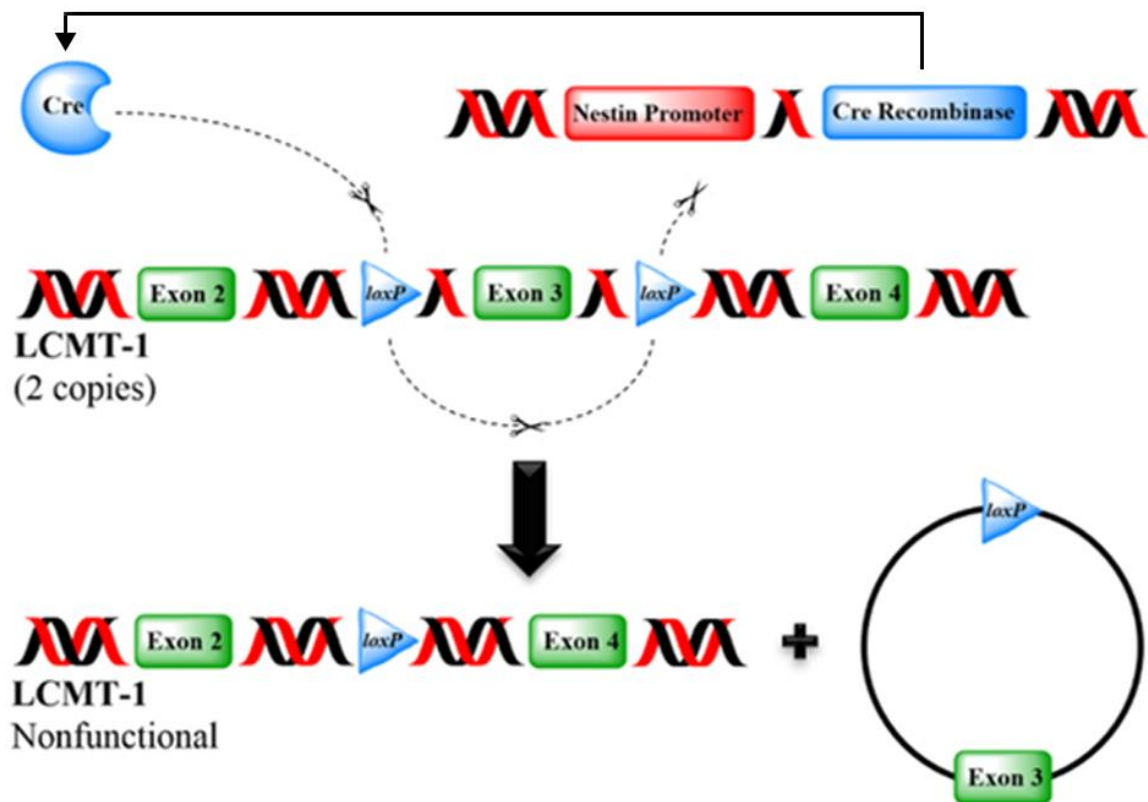
Figure S1. The neuronal-conditional knockout of LCMT-1 using the cre/*loxP* system. The Cre used was *Nestin-Cre* (B6.Cg-Tg(Nes-cre)1Kln/J), a Cre that expresses in neuronal subsets—the nestin promoter is only activated in neuronal and glial cell precursors.
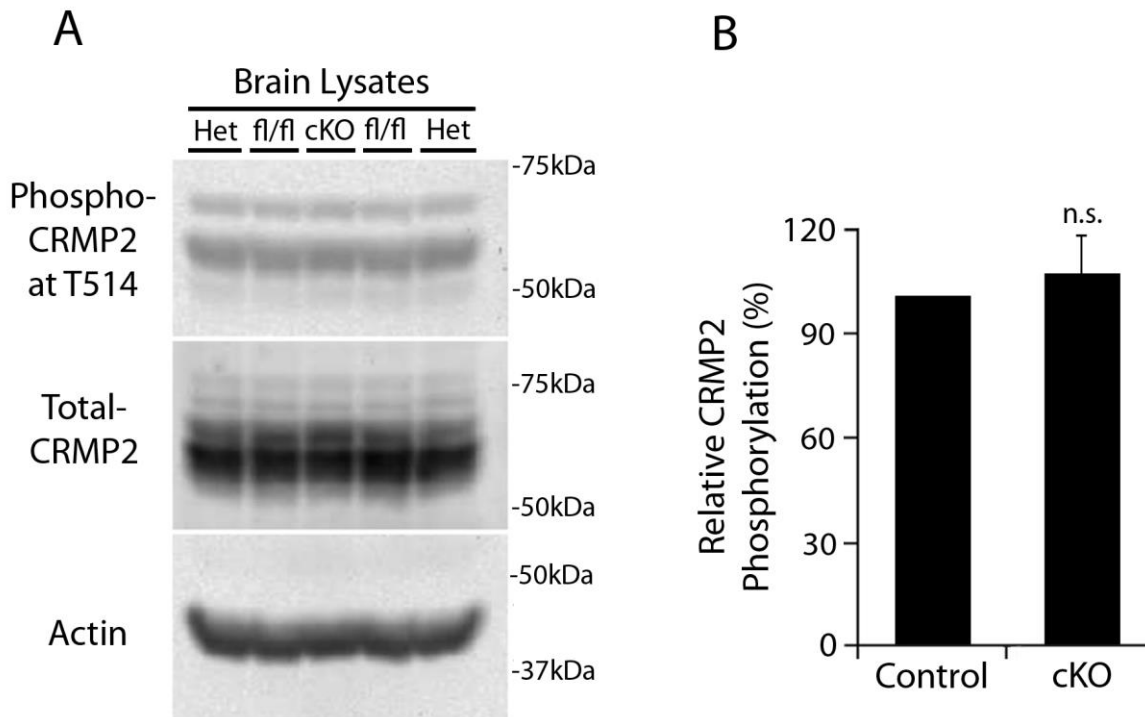
Figure S2. LCMT-1 cKO mice do not show increased phosphorylation of CRMP2 at T514. cKO = NesCre[+/cre] LCMT-1 [flox/flox], Het = NesCre[+/cre] LCMT-1 [+/flox], and fl/fl = NesCre^{+/+} LCMT-1 [flox/flox]. Control = Het or fl/fl. **(A)** CRMP2 phosphorylation is unchanged in cKO mice. P0 mouse pups were euthanized and their brains were homogenized in lysis buffer, and lysates cleared. These samples were run on an SDS-PAGE gel, transferred to a nitrocellulose membrane, and probed with pCRMP2 at T514, tCRMP2, and actin antibodies. **(B)** After quantification and normalizing each lane to actin, phosphorylated CRMP2 signal was divided by total CRMP2 signal. This graph represents the average and standard deviation (error bars) from 3 experiments (3 litters: 7 cKOs and 9 controls in total) of cKO phosphorylation as a % of controls.